This article was downloaded by: [130.126.162.126] On: 16 August 2022, At: 10:49 Publisher: Institute for Operations Research and the Management Sciences (INFORMS)

INFORMS is located in Maryland, USA



Operations Research

Publication details, including instructions for authors and subscription information: http://pubsonline.informs.org

On Solving a Class of Continuous Traffic Equilibrium Problems and Planning Facility Location Under Congestion

Zhaodong Wang, Yanfeng Ouyang, Ruifeng She

To cite this article:

Zhaodong Wang, Yanfeng Ouyang, Ruifeng She (2022) On Solving a Class of Continuous Traffic Equilibrium Problems and Planning Facility Location Under Congestion. Operations Research 70(3):1465-1484. https://doi.org/10.1287/opre.2021.2213

Full terms and conditions of use: https://pubsonline.informs.org/Publications/Librarians-Portal/PubsOnLine-Terms-and-**Conditions**

This article may be used only for the purposes of research, teaching, and/or private study. Commercial use or systematic downloading (by robots or other automatic processes) is prohibited without explicit Publisher approval, unless otherwise noted. For more information, contact permissions@informs.org.

The Publisher does not warrant or quarantee the article's accuracy, completeness, merchantability, fitness for a particular purpose, or non-infringement. Descriptions of, or references to, products or publications, or inclusion of an advertisement in this article, neither constitutes nor implies a quarantee, endorsement, or support of claims made of that product, publication, or service.

Copyright © 2022, INFORMS

Please scroll down for article-it is on subsequent pages



With 12,500 members from nearly 90 countries, INFORMS is the largest international association of operations research (O.R.) and analytics professionals and students. INFORMS provides unique networking and learning opportunities for individual professionals, and organizations of all types and sizes, to better understand and use O.R. and analytics tools and methods to transform strategic visions and achieve better outcomes.

For more information on INFORMS, its publications, membership, or meetings visit http://www.informs.org



OPERATIONS RESEARCH

Vol. 70, No. 3, May-June 2022, pp. 1465-1484 ISSN 0030-364X (print), ISSN 1526-5463 (online)

Contextual Areas

On Solving a Class of Continuous Traffic Equilibrium Problems and Planning Facility Location Under Congestion

Zhaodong Wang,^a Yanfeng Ouyang,^{b,*} Ruifeng She^b

^a Netflix Inc., Los Gatos, California 95032; ^b Department of Civil and Environmental Engineering, University of Illinois at Urbana-Champaign, Urbana, Illinois 61801

*Corresponding author

Received: October 5, 2016

Revised: June 23, 2018; November 29, 2019;

June 3, 2021

Accepted: July 29, 2021

Published Online in Articles in Advance:

March 21, 2022

Area of Review: Transportation

https://doi.org/10.1287/opre.2021.2213

Copyright: © 2022 INFORMS

Abstract. This paper presents methods to obtain analytical solutions to a class of continuous traffic equilibrium problems, where continuously distributed customers from a bounded two-dimensional service region seek service from one of several discretely located facilities via the least congested travel path. We show that under certain conditions, the traffic flux at equilibrium, which is governed by a set of partial differential equations, can be decomposed with respect to each facility and solved analytically. This finding paves the foundation for an efficient solution scheme. Closed-form solution to the equilibrium problem can be obtained readily when the service region has a certain regular shape, or through an additional conformal mapping if the service region has an arbitrary simply connected shape. These results shed light on some interesting properties of traffic equilibrium in a continuous space. This paper also discusses how service facility locations can be easily optimized by incorporating analytical formulas for the total generalized cost of spatially distributed customers under congestion. Examples of application contexts include gates or booths for pedestrian traffic, as well as launching sites for air vehicles. Numerical examples are used to show the superiority of the proposed optimization framework, in terms of both solution quality and computation time, as compared with traditional approaches based on discrete mathematical programming and partial differential equation solution methods. An example with the metro station entrances at the Beijing Railway Station is also presented to illustrate the usefulness of the proposed traffic equilibrium and location design models.

Funding: This work was supported by the U.S. National Science Foundation, Division of Civil, Mechanical, and Manufacturing Innovation [Grants 1234085 and 1662825], and a grant from the USDOT Region V University Transportation Center.

Supplemental Material: The source code (in MATLAB and Python scripts) and data (configuration files, numerical results, and setup files for Viswalk simulations) needed to reproduce the results in the paper are available at https://doi.org/10.1287/opre.2021.2213.

Keywords:facility location • traffic equilibrium • partial differential equation • Neumann problem • conformal mapping

1. Introduction

The transportation community has long recognized the need to address congestion and equilibrium while planning facilities to serve spatially distributed customers. The customers' choices on service facilities and access paths may be coupled with one another due to induced or altered traffic congestion near these facilities. Disregarding the congestion effect while planning facility locations may lead to unnecessarily high transportation cost and negative socio-economic impacts on the general public. In a broader sense, the societal cost includes not only wasted time due to extra delay, but also security and safety hazards.

Examples of such problems can be found in many contexts that involve self-organized traffic in a continuous

space. In the context of pedestrian traffic, crowd congestion not only leads to wasted time due to delay, but also discomfort and safety hazards due to inadequate service facilities (e.g., stairs, exits, and entrances) and lack of flow channelization in open space. Extreme manifestation of such negative consequences of congestion includes the series of devastating pedestrian stampede incidents in recent years, for example, Shanghai's New Year Eve crash in 2014 that killed 36 people and severely injured 47 others (BBC News 2015), and the 2015 Hajj pilgrimage incident in Mina, Saudi Arabia, that killed at least 2,411 pilgrims (Gladstone 2015). In many parts of the world, air vehicles are being considered as an option to allow future travelers to use low-altitude air space. Uber has unveiled a prototype of its UberAIR concept flying

cars that will operate commercially in 2023 (Chow 2018). At the same time, air taxis are being tested in Dubai and China as well (Baggaley 2017, Toh and Ostrower 2018). The freight industry (e.g., Amazon, DHL) has also been exploring the possibility of using short-range unmanned aerial vehicles (i.e., drones) to deliver parcels from a mobile dispatch base (either ground or air based) near customer neighborhoods. The concentration of air vehicle or drone traffic in certain air space (e.g., near the city center or dispatch base) may cause delay and mandate traffic diversion, which in turn significantly affects operational and energy efficiency (She and Ouyang 2021). For example, each Skyport of UberAIR flying cars (providing passenger pickup/dropoff and aircraft battery charging services) are intended to accommodate 200 lift offs and landings each hour (Reisinger 2018), which, if deployed, would cause significant congestion in low-altitude air space. Similar issues would appear in military operations associated with the stationing of aircraft carriers in hostile environments. Even in a seemingly unrelated context, deployment of surveillance sensors (e.g., those based on radiation) in open or constrained spaces (e.g., airports or city squares) may be formulated into a similar problem, if sensor detection effectiveness is affected by not only distance but also blockage effects from a dense crowd—the overall latency and/or reliability of the sensor signals may depend on the path that involves the least cumulation of local blockage. In these and many other similar application contexts, a better understanding of the congestion effect in the continuous space around service facilities will be extremely beneficial for planners to design a more optimized system of such facilities and to minimize the negative impact of congestion.

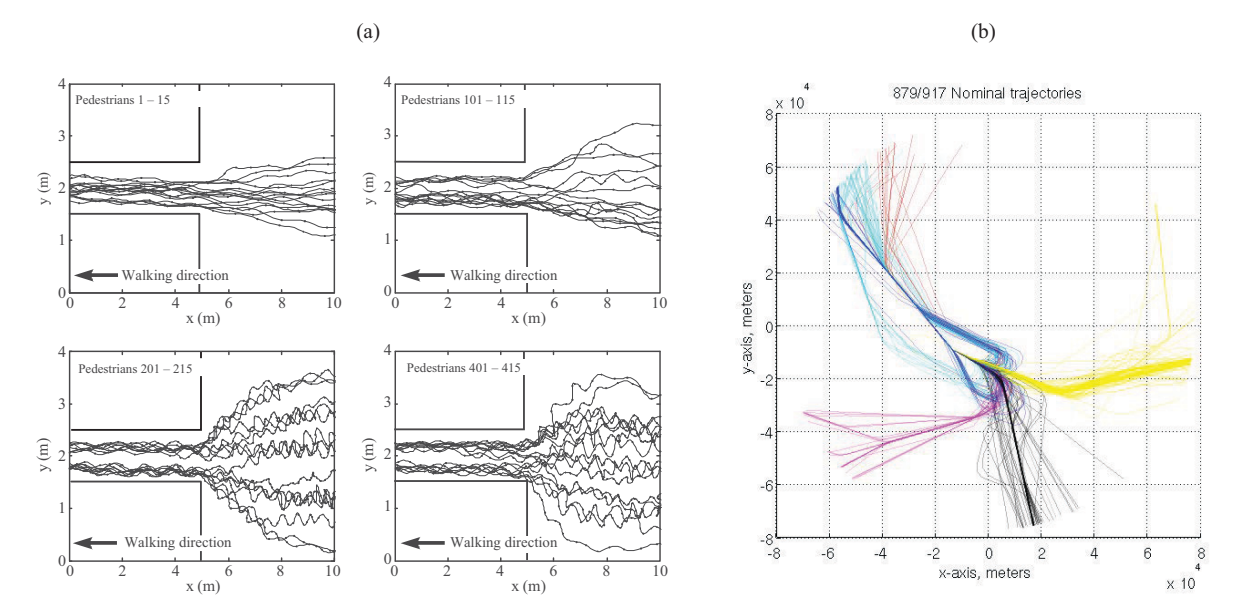
Traffic equilibrium in a continuous space is unique because traveling objects (e.g., air vehicles and pedestrians) follow no clear spatial guideways, select arbitrary travel paths that often deviate from straight lines, and interact with one another from all directions in local neighborhoods. Field experiments in Hoogendoorn and Daamen (2005) show that pedestrians use varying curvy paths to avoid congested areas even if the walking distance is longer, as shown in Figure 1(a). Similarly, air traffic trajectories in Figure 1(b) show similar curvy paths in the air when they concentrate on the landing points. On solving facility location problems in continuous space, Carlsson and Jia (2015) proposed an approach by finding the asymptotically optimal configurations of facilities and spatial partitions. The framework was also applied to find the optimal hub-and-spoke network design in continuous Euclidean space (Carlsson and Jia 2013). However, the impact of traffic congestion was not factored in those models—instead, most of the efforts on traffic congestion have been addressing equilibrium in a discrete network. For example, facility location and

network design problems are often handled as bilevel models with embedded static or dynamic traffic assignment (DTA) problems. Interested readers are referred to Long and Szeto (2019) on dynamic traffic equilibrium and system optimal problem in the discrete setting.

Many studies have addressed the impact of traffic congestion on service network planning, but most of the existing models were developed over an underlying discrete transportation network (Mahmassani and Chen 1993, Peeta and Mahmassani 1995, Jiang et al. 2011), for example, in the context of network design (Abdelghany et al. 2012, Feng and Miller-Hooks 2014), facility location design (Bai et al. 2011, Hajibabai and Ouyang 2013, Hajibabai et al. 2014, Bai et al. 2016), shelter network design problems (Sherali et al. 1991, Li et al. 2012, An et al. 2015), competitive supply chains (Konur and Geunes 2011, 2012), (as well as) planning large public spaces (Gao et al. 2014). Using discrete network flow (even on a very dense network) to approximate traffic concentration and congestion in a continuous space may not always be satisfactory due, in part, to difficulties associated with (i) the coupling of congestion experienced by neighboring travelers in different travel directions, which, in the discrete network model, would have been treated as complex link spillover effects, and (ii) clustering of two-dimensional fluxes into one-dimensional link flows and characterization of link capacities, which are nontrivial tasks. As a result, alternative modeling approaches that can directly describe traffic in a two-dimensional continuous space have gained attention. Helbing et al. (2005) used the social force model to describe pedestrian flows and proposed design solutions to improve the efficiency and safety in congestion-prone areas, such as airport terminals. Yang et al. (1994), Yang (1996), and Yang and Wong (2000) first formulated a series of continuous user traffic equilibrium problems in the form of two-dimensional partial differential equations (PDEs). More recently, a series of extensions has been made to address multiple variants to the problem (Wong and Sun 2001, Ho et al. 2003, Ho and Wong 2005).

Mathematically, suppose that M discrete facilities are built in a bounded and simply connected service region $\Omega \subset \mathbb{R}^2$ to serve continuously distributed customers described by a bounded demand density $q(x) \geq 0, x \in \Omega$. The facilities are located at $x_1, \ldots, x_M \in \Omega$. Facility $i \in \{1, \ldots, M\}$ occupies an infinitesimal circular area $B_i = \{x : |x - x_i| \leq r_0\}$, where $0 < r_0 \ll \sqrt{|\Omega|}$. We assume that the facilities are well separated in the sense that $B_i \cap B_j = \emptyset$ for all $i \neq j$ and $B_i \subset \Omega$ for all i. We define $A_i \subset \Omega$ as the subset of customers who travel to facility i for service. The transportation cost per unit distance per unit demand near location $x \in \Omega$ is isotopic but dependent on the local traffic, that is, $c(x, \mathbf{f}(x))$, where $\mathbf{f}(x)$ is a continuously differentiable

Figure 1. (Color online) Example Pedestrian (a) and Aircraft (b) Trajectories



Sources. Hoogendoorn and Daamen 2005 (a); Gariel et al. 2011 (b).

Notes. (a) Pedestrian trajectories in an empirical experiment with a narrow bottleneck. The lower two scenarios show congestion, and it can be observed that people travel along curvy paths of the continuous space. (b) Aircraft trajectories for landing at SFO (a two-dimensional projection) in one day. Similarly, aircrafts move in all directions along curvy paths in a three-dimensional continuous space.

vector field denoting the flux vector near x. Facility i charges a service fee per unit demand, $C_i(Q_i)$, based on the total flow throughput, $Q_i := \int_{A_i} q(x) dx \ge 0$.

A customer at x chooses to patronize one of the facilities, say facility i, along the best travel path $p(x) \subseteq \mathbb{R}^2$ such that its generalized cost (i.e., sum of travel cost and service fee) is minimized, that is, $x \in \mathcal{A}_i$ if $x_i \in p(x)$ and $[i, p(x)] = \arg\min_{i', p'} \int_{p'(x)} c(x', \mathbf{f}(x')) \, \mathrm{d}x' + C_{i'}(Q_{i'})$. Self-

interested customers may collectively form user equilibrium in the continuous region, such that all customers from location x will experience an equal total generalized cost for obtaining service, which we denote by a scalar function $\phi(x) = \int_{p(x)} c(x', \mathbf{f}(x')) \, \mathrm{d}x' + C_i(Q_i), \ \forall \ x \in \mathcal{A}_i.^2$ Based on Yang and Wong (2000), the traffic equilibrium can be described by the following two-dimensional first-order PDE:

$$\nabla \cdot \mathbf{f}(x) = q(x), \quad x \in \Omega \setminus \bigcup_{i=1}^{M} B_i,$$
 (1a)

$$c(x, \mathbf{f}(x)) \frac{\mathbf{f}(x)}{|\mathbf{f}(x)|} = -\nabla \phi(x), \quad x \in \Omega \setminus \bigcup_{i=1}^{M} B_i,$$
 (1b)

$$\mathbf{f}(x) \cdot \mathbf{n}_x = 0, \quad x \in \partial \Omega,$$
 (1c)

$$\phi(x) = C_i(Q_i), \quad x \in \partial B_i, \quad 1 \le i \le M, \quad (1d)$$

$$\int_{\partial B_i} \mathbf{f}(x) \cdot \mathbf{n}_x \, \mathrm{d}x + Q_i = 0, \qquad 1 \le i \le M, \quad \text{(1e)}$$

where $\nabla \cdot$ is the divergence operator; ∇ is the gradient operator; $\partial \Omega$ and ∂B_i denote the boundaries of Ω and B_i , respectively; \mathbf{n}_x denotes the outward unit normal vector to the boundary at $x \in \partial \Omega$ or $x \in \partial B_i$. Equations (1a) and (1e) follow flux conservation; (1b) guarantees

that the customers will choose their cost-minimizing travel paths; (1c) implies that no traffic crosses the boundary of the region; and (1d) directly follows the definition of $\phi(x)$ at facility boundaries.

The solution to the previous PDEs has been incorporated into upper level optimization models for a number of application contexts, for example, point service facility location design (Ouyang et al. 2015), reliable location design (Wang et al. 2021), guideway network design (Zhang et al. 2021), and truck-drone distribution system design (Wang and Ouyang 2018). In particular, point service facilities could be gates or booths for pedestrians, dispatch bases or Skyports for drones, or even surveillance sensors at airports. The facility location design can be optimized in many ways, for example, the problem could be written into the following median-type formulation:

$$\min_{M,x} \quad \bar{\phi} \tag{2a}$$

subject to (1) and
$$\sum_{i=1}^{M} g(x_i) \leq \mathcal{B}, \tag{2b}$$

where g(x) is the cost for opening a facility at x, (2b) is the budget constraint, and $\bar{\phi} = \left[\int_{\Omega} q(x) \, \mathrm{d}x \right]^{-1} \int_{\Omega} \phi(x) \, dx$ is the average customer service cost.

The previous model includes nonlinear differential equations as part of the constraints and hence is very difficult to solve. Such problems are typically solved by numerical methods (e.g., finite element method, or

FEM) that seek approximation in a set of local partitions (i.e., finite elements) that can be systematically integrated into a global system of equations (Yang and Wong 2000, Wong et al. 2004, Ho and Wong 2006, Du et al. 2016). Embedding such PDEs as constraints in an upper level optimization problem typically requires iterative algorithms (such as Lagrangian relaxation; see Ouyang et al. 2015) that solve the PDEs many times. With the standard PDE solution methods (e.g., via FEM), this incurs prohibitive computational burdens. Yet, little efforts have been made toward investigating the structure of the PDEs in the hope to obtain closed-form analytical solutions, such that the PDEs' solution can be effectively used to plan service facilities. In light of this, this paper focuses on developing analytical solution methods for a class of continuous traffic equilibrium problems. We show that under certain conditions, the previous PDEs can be asymptotically solved in closed forms when the sizes of facilities are negligible as compared with the service region size, for specially shaped service regions (e.g., circular areas). For more generally shaped regions, an additional conformal mapping treatment (which can also be expressed in closed forms) is needed. Our PDE solution will not only serve as an efficient way to compute congestion effects in various application contexts, but also shed light on some basic properties of continuous traffic equilibrium in a twodimensional space. For example, we show that the size of the facilities has a significant impact on the equilibrium flux pattern, and we discuss the limiting behavior when the size of the facilities approaches zero. Formulas for calculating the total generalized cost for all customers as well as the flow throughput at each facility are developed; this brings in significant computation advantages over the traditional numerical methods in the literature. These analytical results can be easily incorporated into optimization models, for example, for planning service facilities to serve spatially distributed customers. In this paper, we directly incorporate the analytical results into a nonlinear solver to solve some simple location optimization problems, which manifests computational gains comparing with the numerical methods developed by Ouyang et al. (2015). The computational methods and modeling tools from this paper will allow transportation planners (e.g., supply chain planners for drone deliveries in Amazon, DHL, and service facilities designers for transit plazas or sport stadiums, or urban mobility service providers such as Uber Elevate) to estimate the congestion cost induced by their designs, and in turn help those planners to design a more optimized system of facilities that minimizes the negative impact of congestion.

The remainder of this paper is organized as follows. The basic PDE solution methodology is presented in Section 2 and Section 3. We start with deriving a PDE solution to a basic problem where all customers go to only one facility for service, which is presented in Section 2. The result serves as the building block for

solving multifacility cases via an exact decomposition scheme in Section 3. Section 4 presents two numerical examples, one on a unit square and the other on an irregular service region. The last section presents concluding remarks.

2. Single Facility

We first consider the special case of problem (1) where only one facility (i.e., M = 1) is built at $x_1 \in \Omega$. In what follows, we first transform the PDE into a solvable form by showing equivalence and then derive the solution explicitly.

To start with, it can be easily verified, following the divergence theorem (Marsden and Tromba 2003),

$$\int_{\Omega} \nabla \cdot \mathbf{f}(x) \, \mathrm{d}x = \oint_{\partial \Omega} \mathbf{f}(x) \cdot \mathbf{n}_x \, \mathrm{d}x,$$

that the vector field determined by the following equation also satisfies (1a) and (1e):

$$\nabla \cdot \mathbf{f}(x) = q(x) - Q\delta(x - x_1), \quad x \in \Omega,$$
 (3)

where $Q = \int_{\Omega} q(x) dx$ and $\delta(\cdot)$ is the Dirac delta function defined on \mathbb{R}^2 .

Next, note that the presence of the cost potential function $\phi(x)$ in (1b) implies that no curl of $\nabla \phi(x)$ exists anywhere; hence, (1b) can be equivalently rewritten as follows: for all $x \in \Omega \setminus B_1$,

$$0 = \nabla \times [-\nabla \phi(x)] = \nabla \times \left[c(x, \mathbf{f}(x)) \frac{\mathbf{f}(x)}{|\mathbf{f}(x)|} \right] = \frac{c(x, \mathbf{f}(x))}{|\mathbf{f}(x)|}$$
$$\nabla \times \mathbf{f}(x) + \nabla \frac{c(x, \mathbf{f}(x))}{|\mathbf{f}(x)|} \times \mathbf{f}(x),$$

where $\nabla \times$ is the curl operator. For nontrivial cases, $\frac{c(x,f(x))}{|f(x)|} \not\equiv 0$, and hence, as long as

$$\nabla \frac{c(x, \mathbf{f}(x))}{|\mathbf{f}(x)|} \times \mathbf{f}(x) = 0, \quad x \in \Omega,$$
 (4)

holds, we know that (1b) reduces to the following:

$$\nabla \times \mathbf{f}(x) = 0, \quad x \in \Omega. \tag{5}$$

There could be many possible ways for condition (4) to hold. The simplest example might be the case when the travel cost function is linear with respect to flux intensity, that is, $c(x, \mathbf{f}(x)) \sim |\mathbf{f}(x)|$. In this paper, we limit our focus to the class of problems where condition (4) holds at least approximately.

When the conservative property (5) is satisfied, we can introduce a new function u(x) such that

$$\nabla u(x) = -\mathbf{f}(x), \quad x \in \Omega, \tag{6}$$

and hence the solution to the following *Neumann problem* in the mathematics literature (Guenther and Lee 1996) must also satisfy (3), (5) and (1c):

$$\Delta u(x) = -q(x) + Q\delta(x - x_1), \quad x \in \Omega, \tag{7a}$$

$$\nabla u(x) \cdot \mathbf{n}_x = 0, \quad x \in \partial \Omega, \tag{7b}$$

where Δ is the Laplacian operator. It is known that the integral representation of the solution to this Neumann problem (7) has the following form:

$$u(x) = \int_{\Omega} N(x', x)q(x') dx' - QN(x_1, x) + \bar{u},$$
 (8)

where \bar{u} is average value of u(x) in region Ω^{5} and N(x',x) is the Neumann function (Roach 1982) defined over two points $x', x \in \Omega$ that uniquely solves the following normalized Neumann problem for all $x' \in \Omega$,

$$-\Delta N(x',x) = \delta(x-x') - \frac{1}{|\Omega|}, \quad x \in \Omega, \tag{9a}$$

$$\nabla N(x', x) \cdot \mathbf{n}_x = 0, \quad x \in \partial \Omega, \tag{9b}$$

$$\int_{\Omega} N(x', x) \, \mathrm{d}x = 0. \tag{9c}$$

It is known that the Neumann function should have the following form:

$$N(x', x) = S(x', x) + U(x', x), \tag{10}$$

where

$$S(x', x) = -\frac{1}{2\pi} \log |x - x'| + \frac{|x|^2}{4 |\Omega|},$$

and U(x',x) as a function of x is harmonic in Ω but has nonhomogeneous Neumann boundary conditions due to (9b), namely,

$$\Delta U(x', x) = 0, \quad x \in \Omega, \tag{11a}$$

$$\nabla U(x',x) \cdot \mathbf{n}_x = -\nabla S(x',x) \cdot \mathbf{n}_x, \quad x \in \partial \Omega.$$
 (11b)

Now we are ready to show that as $r_0 \rightarrow 0^+$, the solution to the Neumann problem also (asymptotically) satisfies (1d). Note from (8) and (10) that in the neighborhood of x_1 , $\log(\cdot)$ monotonically increases with no upper bound. Let $B = \{x': |x' - x| \le r\} \supseteq \Omega$ be a disk centered at x, where radius r is sufficiently large such that the first inequality below holds. Then we have

$$\int_{\Omega} \frac{1}{2\pi} \log|x' - x| \, dx' \le \int_{B} \frac{1}{2\pi} \log|x' - x| \, dx'$$
$$= r^{2} (2 \log r - 1)/4 < \infty, \quad x \in \Omega.$$

Therefore, for bounded demand density, that is, $\sup_{x' \in \Omega}$ $q(x') < \infty$, we have $\int_{\Omega} S(x', x) q(x') dx' < \infty$ and continuous as well. Then, $\lim_{x\to x_1}\int_{\Omega} S(x',x)q(x')$ $dx'=\int_{\Omega} S(x',x)q(x')$ $(x', x_1) q(x') dx' < \infty$. Moreover, because U(x', x) is harmonic, its regularity and the maximum principle implies that $\lim_{x\to x_1} U(x_1,x) = U(x_1,x_1) < \infty$ and $\lim_{x\to x_1} U(x_1,x_2) = U(x_1,x_2) < \infty$ $\int_{\Omega}U(x',x)q(x')\,\mathrm{d}x'=\int_{\Omega}U(x',x_1)q(x')\,\mathrm{d}x'<\infty. \text{ As a result,}$ $\lim_{x\to x_1} \int_{\Omega} N(x',x) q(x') dx' = \int_{\Omega} N(x',x_1) \quad q(x') dx' < \infty. \quad \text{To}$

 $\lim_{x \to x_1} u(x) = \lim_{r_0 \to 0} \frac{Q}{2\pi} \log r_0 + \int_{\Omega} N(x', x_1) q(x') \, dx'$

 $-QU(x_1,x_1)-\frac{Q|x_1|^2}{4|\Omega|}+\bar{u},$ (12) which is independent of x and dominated by the first term, implying that f(x) near x_1 is asymptotically perpendicular to the boundary ∂B_1 as $r_0 \to 0^+$. Therefore, (1d) is satisfied based on the gradient theorem (Williamson and Trotter 1996).

Recall that (3) implies (1a) and (1e),⁶ and (5) is equivalent to (1b). Hence, the Neumann problem solution from (8), which therefore satisfies (3), (5), (1c), and (1d) in light of (6), also solves the original problem (1) asymptotically as $r_0 \rightarrow 0^+$. This is stated in the following proposition.

Proposition 1. As $r_0 \rightarrow 0^+$ and M = 1, when (4) holds, the solution f(x) to (1) can be asymptotically obtained from (8) via $\mathbf{f}(x) = -\nabla u(x)$, $\forall x$.

Now, the solution to continuous traffic equilibrium reduces to one on finding the Neumann function for Ω . It turns out that the specific form of the Neumann function depends on the shape of the region Ω . For certain special shapes, Neumann functions can be expressed in explicit closed forms; some examples will be given in Section 2.1. However, for a generally shaped region Ω , it may not be possible to directly express the Neumann functions in closed forms. In such cases, we either resort to numerical solutions or conduct spatial mapping to change the shape of the region. The latter approach is discussed in Section 2.2.

2.1. Service Region with Special Shapes

Over the years, the applied mathematics community has found closed-form Neumann functions for some specific regions, including circular disks, rectangles, and equilateral triangles (McCartin 2011). For the sake of brevity, we present these Neumann functions without proof. Interested readers are encouraged to verify that these closed-form functions indeed solve the Neumann problem described in the previous section.

2.1.1. Unit Disk. When Ω is the unit disk, $\{x: |x| \leq 1\}$, the corresponding Neumann function is well known (Kolokolnikov et al. 2005):

$$N(x',x) = \frac{1}{2\pi} \left(-\log|x - x'| - \log|x|x'| - \frac{x'}{|x'|} + \frac{|x|^2 + |x'|^2}{2} - \frac{3}{4} \right)$$
(13)

Figure 2, (a) and (b) show, respectively, the flux pattern and cost surface based on (8) and (13) when $c(x, \mathbf{f}(x)) = |\mathbf{f}(x)|, q(x) \equiv 1 \text{ and } x_1 = (\frac{1}{2}, 0)$

2.1.2. Rectangle. For a rectangular region $\Omega = [0, a] \times$ [0,b], where a,b>0, the Neumann function can be expressed by a trigonometric series (Roach 1982):

$$N(x',x) = \frac{4}{ah}$$

$$\sum_{m=m=0}^{\infty} \gamma_{mn} \frac{\cos(m\pi x^{(1)}/a)\cos(m\pi x'(1)/a)\cos(n\pi x^{(2)}/b)\cos(n\pi x'(2)/b)}{\pi^2(m^2/a^2+n^2/b^2)}$$

(14)

where $(x^{(1)}, x^{(2)})$ and $(x'^{(1)}, x'^{(2)})$ are the coordinates of points x and x', respectively; $\gamma_{00} = 0$, $\gamma_{m0} = \gamma_{0n} = \frac{1}{2}$ and $\gamma_{mn} = 1$ for m > 0, n > 0.

Figure 2, (c) and (d) show the flux pattern and cost surface when $c(x, \mathbf{f}(x)) = |\mathbf{f}(x)|$, $q(x) \equiv 1$, a = b = 1 and $x_1 = \left(\frac{3}{4}, \frac{1}{2}\right)$.

2.2. Service Region with General Shapes

For an arbitrary bounded region Ω , the Neumann function is not readily available, but it still follows the basic form (10). We propose to use conformal mapping (Henrici 1993) to help transform the arbitrarily shaped region to one in which (11) can be solved in closed forms.

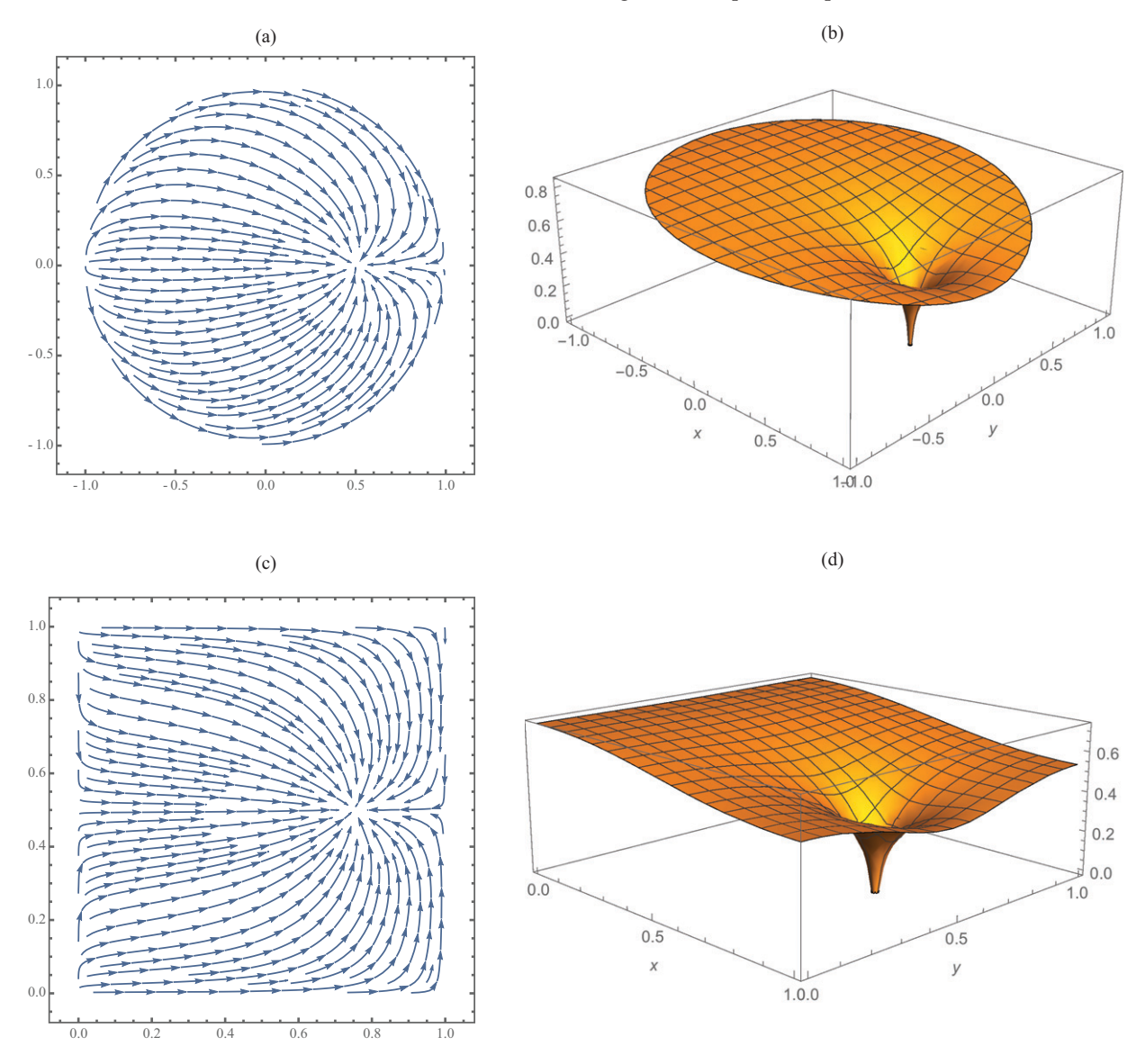
In so doing, we use the complex plane $\mathbb C$ to represent the two-dimensional space, and map the points in Ω to those in another region $D \subset \mathbb C$ while preserving angles, that is, the mapping is denoted as $h:\Omega \to D$, where $\Omega,D \subset \mathbb C$. Because harmonic functions remain harmonic under conformal mapping, we can obtain the following immediate result.

Proposition 2. Let $x \in \Omega$ and $\zeta = h(x) \in D$ be a one-to-one conformal mapping from region Ω to region D, which is also continuous on the boundary $h: \partial\Omega \to \partial D$. Let h'(x) be the differential of the mapping at x. Suppose $H(x', \zeta)$ is a harmonic function of ζ in D satisfying

$$\Delta H(x',\zeta) = 0, \quad \zeta \in D,$$
 (15a)

$$\nabla H(x',\zeta) \cdot \mathbf{n}_{\zeta} = -|h'(x)|^{-1} \nabla S(x',x) \cdot \mathbf{n}_{x}, \quad \zeta \in \partial D. \quad (15b)$$

Figure 2. (Color online) Flux Pattern and Cost Surface for Service Regions with Special Shapes



Note. (a) Flux pattern: circular disk; (b) cost contour; circular disk; (c) flux pattern: square; and (d) cost contour: square.

Then, U(x',x) = H(x',h(x)) is the solution to Equation (11) on region Ω .

Proof. Because $H(x',\zeta)$ is a harmonic function of ζ that remains harmonic under conformal mapping, we immediately know U(x',x) is also harmonic and hence (11a) is satisfied. Moreover, if ζ and x are the corresponding points on ∂D and $\partial \Omega$, respectively, we have, in view of the conformality:

$$\nabla U(x',x) \cdot \mathbf{n}_x = [|h'(x)| \cdot \nabla H(x',\zeta)] \cdot \mathbf{n}_\zeta = |h'(x)|$$
$$\nabla H(x',\zeta) \cdot \mathbf{n}_\zeta.$$

Hence, (11b) also is satisfied. This completes the proof. \Box

Proposition 2 has an important implication on solving the Neumann problem for irregularly shaped regions. Now that we know the Neumann function on a circular disk, we can set D to be a unit disk and produce the Neumann function for any other simply connected region $\Omega \subsetneq \mathbb{C}$.

Corollary 1. Let $\zeta = h(x)$ denote a conformal mapping that transforms a point in a simply connected region $x \in \Omega$ into one in the unit disk $\zeta \in D$. Then the Neumann function on Ω is given by (10) where

$$U(x',x) = -\frac{1}{\pi} \int_0^{2\pi} (\log |e^{j\theta} - h(x)|) \cdot |h'(h^{-1}(e^{j\theta}))|^{-1} \nabla S(x',h^{-1}(e^{j\theta})) \cdot \mathbf{n}_{h^{-1}(e^{j\theta})} d\theta + \chi,$$
(16)

where $j = \sqrt{-1}$, e is the base of the natural logarithm, and χ is a scalar chosen so that (9c) is satisfied.

Proof. We first note that h(x) must exist due to Riemann mapping theorem (Ahlfors 1966). Then, in the unit disk D, by Dini's formula (Henrici 1993), the solution to (15) is

$$H(x',\zeta) = -\frac{1}{\pi} \int_0^{2\pi} (\log |e^{j\theta} - \zeta|)$$
$$\cdot |h'(x)|^{-1} \nabla S(x',x) \cdot \mathbf{n}_x \, \mathrm{d}\theta + \chi,$$

where $x = h^{-1}(e^{i\theta})$. Noting that U(x', x) = H(x', h(x)), we have completed the proof. \square

Corollary 1 provides an efficient formula to evaluate the Neumann function for regions with general shapes. If the conformal mapping function h, its inverse h^{-1} as well as its derivative h' can be explicitly expressed, (16) can be directly applied. In practical applications, if the region boundary is given without parametrized expression, the numerical conformal mapping would be applied to efficiently evaluate the cost potential. As stated in Papamichael and Stylianopoulos (2010), numerical approximated conformal mapping h and its inverse h^{-1} can be efficiently evaluated by many public domain software packages. The derivative h' would also be evaluated using basic numerical methods. Although the extra numerical computation for the

conformal mapping may induce extra computational costs, our framework still has the advantage over the finite elemental method in practical applications. Note that the conformal mapping only depends on the shape of the domain boundary, so it can be precomputed and stored. In Ouyang et al. (2015), for each set of location configuration, triangular finite element meshes must be regenerated again to evaluate the average costs—this involves heavy computational costs. In contrast, using our conformal mapping based method, for any facility location configuration, we can directly use Equation (15), without any extra computation, to efficiently estimate the average cost. This significantly reduces the computational burden. In our follow-up paper (Wang et al. 2021), the advantage of the proposed conformal mapping method would be further magnified when considering facility location design under disruption uncertainties.

3. Multiple Facilities

3.1. Decomposition Scheme

Now, we extend the discussion to the case of M > 1 facilities that compete for self-organized demand, where the one-facility results from the previous section will serve as a building block. Recall that if (4) holds, then (1b) becomes (5), and then all the differential equations in (1) become linear with respect to $\mathbf{f}(x)$. In light of this, we will next show that the solution to (1) for M > 1 facilities, described by the vector field $\mathbf{f}(x)$, should be expressed as the superposition of M vector fields $\mathbf{f}_i(x)$, for $1 \le i \le M$, each corresponding to a single facility and satisfying

$$\nabla \cdot \mathbf{f}_i(x) = \frac{Q_i}{Q} q(x) - Q_i \delta(x - x_i), \quad 1 \le i \le M, x \in \Omega, \quad (17a)$$

$$\nabla \times \mathbf{f}_i(x) = 0, \quad 1 \le i \le M, x \in \Omega, \tag{17b}$$

$$\mathbf{f}_i(x) \cdot \mathbf{n}_x = 0, \quad 1 \le i \le M, x \in \partial \Omega.$$
 (17c)

Equation (17) is essentially the equivalent of (3), (5) and (1c) for an arbitrary facility i, if we imagine (that the total demand served by this facility), Q_i , comes proportionally from every neighborhood, that is, facility i attracts demand with a density $q(x)Q_i/Q$ from x. Note that Q_i/Q is used only as a weight factor in the revealed solution structure when we superimpose the multiple vector fields. Each weight factor is solved as an unknown such that the boundary conditions will hold. Because each imaginary sub-flux $f_i(x)$ is a vector field, eventually, for any point x, the actual flux $\mathbf{f}(x)$ at a location x is the vector summation of multiple $f_i(x)$'s using those weight factors, which in the end shall have only one direction. As such, all the demand from location x would eventually flow toward this direction and choose the facility corresponding to it. Per our discussion in the previous section, each of these PDEs can be solved similarly via the Neumann function as follows:

$$u_{i}(x) = \frac{Q_{i}}{Q} \int_{\Omega} N(x', x) q(x') dx' - Q_{i} N(x_{i}, x) + \bar{u}_{i}, \quad (18)$$

where $\nabla u_i(x) = -\mathbf{f}_i(x)$ for $1 \le i \le M$.

It is easy to verify that the resultant flux $\mathbf{f}(x) = \sum_{i=1}^{M} \mathbf{f}_i(x)$ satisfies (3), the equivalent of (1a) and (1e), because of the following:

$$\nabla \cdot \mathbf{f}(x) = \sum_{i=1}^{M} \nabla \cdot \mathbf{f}_i(x) = q(x) - \sum_{i=1}^{M} Q_i \delta(x - x_i), \quad x \in \Omega.$$

Moreover, when (4) holds, (1b) is satisfied because

$$\nabla \times \left(c(x, \mathbf{f}(x)) \frac{\mathbf{f}(x)}{|\mathbf{f}(x)|} \right) = \frac{c(x, \mathbf{f}(x))}{|\mathbf{f}(x)|} \nabla \times \mathbf{f}(x)$$
$$= \frac{c(x, \mathbf{f}(x))}{|\mathbf{f}(x)|} \sum_{i=1}^{M} \nabla \times \mathbf{f}_{i}(x) = 0,$$

and (1c) holds as $\mathbf{f}(x) \cdot \mathbf{n}_x = \sum_{i=1}^{M} \mathbf{f}_i(x) \cdot \mathbf{n}_x = 0$.

Recall the case for one facility, from (12) we know that in the neighborhood of the facility, the flux tends to be perpendicular to the boundary of the facility, and its magnitude approaches infinity. In the multifacility case, as long as these facilities are well separated, this situation applies to each facility, and hence the total flux near a facility is dominated by that entering this facility, that is, $\mathbf{f}(x) = \sum_{i=1}^{M} \mathbf{f}_i(x) \approx \mathbf{f}_i(x)$ for all $x \in \partial B_i$, and this flux is approximately perpendicular to ∂B_i . As such, (1d) is satisfied based on the gradient theorem and the fact that $\mathbf{f}(x)$ is curl free as long as the following equations hold:

$$C_{i}(Q_{i}) - C_{i-1}(Q_{i-1}) = \int_{\widetilde{x}_{i} \to \widetilde{x}_{i-1}} \frac{c(x, \mathbf{f}(x))}{|\mathbf{f}(x)|} \mathbf{f}(x) \cdot \mathbf{t}_{x} dx,$$

$$2 \le i \le M, \quad (19)$$

where the integral is defined over a Jordan arc passing from an arbitrary $\tilde{x}_i \in \partial B_i$ to an arbitrary $\tilde{x}_{i-1} \in \partial B_{i-1}$ excluding B_1, \ldots, B_M , and \mathbf{t}_x is the tangent vector along the arc at location x. The results are summarized in the following proposition.

Proposition 3. When (4) holds and in the limit as $r_0 \to 0^+$, the solution $\mathbf{f}(x)$ to (1) can be asymptotically expressed as the superposition of M continuously differentiable vector fields $\mathbf{f}_1(x), \ldots, \mathbf{f}_M(x)$ for all $x \in \Omega$, that is, $\mathbf{f}(x) = \sum_{i=1}^M \mathbf{f}_i(x)$, where the M vector fields are determined by (18), (19), and $Q = \sum_{i=1}^M Q_i$.

Proposition 3 provides a decomposition scheme for solving continuous traffic equilibrium with multiple facilities. In the preceding section, we presented ways to obtain the closed-form Neumann functions for one facility. Substituting the Neumann functions into (18) yields the equilibrium flux pattern for each facility i individually, and the flux will be scaled by a factor of Q_i/Q . By solving a system of Equation (19), we can obtain the throughput at each facility, Q_i , and hence retrieve $\mathbf{f}(x)$ for multiple facilities by superimposing the vector fields $\mathbf{f}_i(x)$ for all i. Note that there are only M-1 independent Q_i 's because $Q = \sum_{i=1}^M Q_i$ is a

constant. The generalized cost $\phi(x)$ can then be obtained from the flux pattern by evaluating (1b) and (1d).

In general, to solve the system of Equation (19), if the line integral on the right-hand side cannot be explicitly expressed, numerical integration is necessary to obtain an evaluation. Due to the possible complexity of the integral, existence and uniqueness of the system (19) is not guaranteed for all possible forms of the congestion function $c(x, \mathbf{f}(x))$. However, if the congestion function is linear, system (19) can be simplified such that a unique solution is guaranteed and many other desirable properties can be explored. This is discussed in the following section.

3.2. Properties of Linear Congestion Functions

If we further assume that the congestion function is linear with respect to local flux intensity, namely, $c(x, \mathbf{f}(x)) \sim |\mathbf{f}(x)|$, the equilibrium solution would have some neat properties. This may provide a rich lode of opportunities for exploring the nature of the continuous traffic equilibrium problem. In what follows, without losing generality, we assume for the sake of simplicity that

$$c(x, \mathbf{f}(x)) = |\mathbf{f}(x)|. \tag{20}$$

In this case, (1b) becomes $f(x) = -\nabla \phi$ and PDEs (1) turn into a Poisson equation with mixed Dirichlet and Neumann boundary conditions. The linearity of gradient operator ∇ implies that $\phi(x)$ differs from $u_1(x) + \cdots + u_M(x)$ at most by a constant. Moreover, (19) can be reduced to

$$C_{i}(Q_{i}) - C_{i-1}(Q_{i-1}) = \sum_{j=1}^{M} [u_{j}(\widetilde{x}_{i}) - u_{j}(\widetilde{x}_{i-1})], \quad 2 \le i \le M,$$
(21)

where $\widetilde{x}_i \in \partial B_i$, $\forall i$. Substituting (18) into (21) yields $C_i(Q_i) - C_{i-1}(Q_{i-1})$

$$= \int_{\Omega} (N(x', \widetilde{x}_i) - N(x', \widetilde{x}_{i-1})) q(x') dx'$$

$$+ \sum_{k=1}^{M} Q_k (N(x_k, \widetilde{x}_{i-1}) - N(x_k, \widetilde{x}_i)), \quad 2 \le i \le M.$$
(22)

The system of Equations (22), along with $\sum_{i=1}^{M} Q_i = Q$, can be used to solve the total flow throughput Q_i , $\forall i$, given the locations of facilities $\mathbf{x} = \{x_1, x_2, \ldots, x_M\}$. Note that this property implies that the cost function $\phi(x), x \in \Omega$ can be directly obtained without solving the flux fields. The following proposition discusses the existence and uniqueness of the solution to the nonlinear system (22).

Proposition 4. The nonlinear system (22), along with $\sum_{i=1}^{M} Q_i = Q$, has a unique solution in the limit as $r_0 \to 0^+$ if $C_i(\cdot)$, $\forall 1 \le i \le M$ are bounded and continuously differentiable.

Proof. Let $P_i = \int_{\Omega} N(x', \tilde{x}_i) q(x') dx'$, then, we can rewrite the nonlinear systems as follows:

$$C_i(Q_i) = P_i - \sum_{k=1}^{M} Q_k N(x_k, \tilde{x}_i) + \kappa, \quad 1 \le i \le M,$$
 (23a)

$$Q = \sum_{k=1}^{M} Q_i, \tag{23b}$$

where κ is an auxiliary variable in addition to Q_i , $\forall i$. As $r_0 \rightarrow 0^+$, we have that

$$N(x_i, \widetilde{x}_j) = \begin{cases} N(x_i, x_j), & i \neq j, \\ -\frac{1}{2\pi} \log r_0 + U(x_i, x_i) + \frac{|x_i|^2}{4 |\Omega|}, & i = j. \end{cases}$$

Let $\varepsilon = -2\pi/\log r_0$, then $\varepsilon \to 0^+$ as $r_0 \to 0^+$. As such, the nonlinear algebraic system (23) can be rewritten in the following form:

$$(I + \varepsilon A)\mathbf{v} = \varepsilon^2 \mathbf{h}(\mathbf{v}), \tag{24}$$

where

$$A = \begin{pmatrix} U(x_1, x_1) + \frac{|x_1|^2}{4 |\Omega|} & N(x_1, x_2) & \cdots & N(x_1, x_M) & -1 \\ N(x_2, x_1) & U(x_2, x_2) + \frac{|x_2|^2}{4 |\Omega|} & \cdots & N(x_1, x_M) & -1 \\ \vdots & \vdots & \ddots & \vdots & \vdots \\ N(x_M, x_1) & \cdots & \cdots & U(x_M, x_M) + \frac{|x_M|^2}{4 |\Omega|} & -1 \\ 1 & \cdots & \cdots & 1 & 0 \end{pmatrix},$$

$$\mathbf{v} = (\varepsilon Q_1, \dots, \varepsilon Q_M, \varepsilon \kappa)^T$$

$$\mathbf{h}(\mathbf{v}) = (P_1 - C_1(Q_1), \dots, P_M - C_M(Q_M), Q + \varepsilon^{-1}\kappa).$$

As $\varepsilon \to 0^+$, $I + \varepsilon A$ must be invertible and the inverse $(I + \varepsilon A)^{-1} = I - \varepsilon A + \varepsilon^2 A^2 + \cdots$. Note that $Q_i \in [0,Q]$, $\forall 1 \le i \le M$ and $\sum_{i=1}^M Q_i = Q$, hence there exists an i' such that $>Q_{i'} \ge Q/M$; otherwise, $\sum_{i=1}^M Q_i < MQ/M = Q$, which is a contradition. For this i', we have that $P_{i'} < \infty$ as $\varepsilon \to 0^+$, it follows from (23a) that $\kappa \sim \mathcal{O}(\varepsilon^{-1})$. Therefore, ignoring the third and higher order terms of ε , (24) can be rewritten in the following form:

$$\mathbf{v} = \mathbf{h}(\mathbf{v}),\tag{25}$$

where

$$\widetilde{\mathbf{h}}(\mathbf{v}) = \varepsilon \begin{pmatrix} \varepsilon \kappa + \varepsilon (P_1 - C_1(Q_1)) - \varepsilon^2 s_1 \kappa \\ \vdots \\ \varepsilon \kappa + \varepsilon (P_M - C_M(Q_M)) - \varepsilon^2 s_M \kappa \\ \kappa + \varepsilon Q - \varepsilon^2 M \kappa \end{pmatrix} + \mathcal{O}(\varepsilon^3),$$
(26)

where $s_i = \sum_{j=1}^{M} (A)_{ij}$. The last row in (25) implies that $\kappa = Q/(M\varepsilon) + \mathcal{O}(1)$. Substituting it into other rows, we obtain that

$$\widetilde{\mathbf{h}}(\mathbf{v}) = \begin{pmatrix} \varepsilon Q/M \\ \vdots \\ \varepsilon Q/M \\ \varepsilon \kappa \end{pmatrix} + \mathcal{O}(\varepsilon^2). \tag{27}$$

Now consider the set $\mathcal{K} := \{\mathbf{v} \in \mathbb{R}^{M+1} : 0 \le v_i \le \varepsilon Q, \forall 1 \le i \le M; v_{M+1} \in J\}$, where J is any closed interval (note that $\varepsilon \kappa \sim Q(1)$). It follows from (27) that as $\varepsilon \to 0$, function $\widetilde{\mathbf{h}}$ maps \mathcal{K} into a strict subset of \mathcal{K} , that is, $\widetilde{\mathbf{h}}(\mathcal{K}) \subset \mathcal{K}$. Because \mathcal{K} is compact and convex, Brouwer's theorem guarantees that existence of $\mathbf{v} \in \mathcal{K}$ with $\widetilde{\mathbf{h}}(\mathbf{v}) = \mathbf{v}$, which implies the existence of the solution to the nonlinear system (22).

Suppose that $\mathbf{v} = (\varepsilon Q_1, \dots, \varepsilon Q_M, \varepsilon \kappa)$ and $\mathbf{v}' = (\varepsilon Q_1', \dots, \varepsilon Q_M', \varepsilon \kappa')$ are two distinct solutions. Then, for $i = 1, \dots, M$, we have from (24) that

$$Q_i + \varepsilon \sum_{i=1}^{M} (A)_{ij} Q_j - \varepsilon \kappa = \varepsilon (P_i - C_i(Q_i)),$$
 (28a)

$$Q_i' + \varepsilon \sum_{j=1}^{M} (A)_{ij} Q_j' - \varepsilon \kappa' = \varepsilon (P_i - C_i(Q_i')).$$
 (28b)

Subtracting (28b) from (28a) yields

$$Q_i - Q_i' = \varepsilon(\kappa - \kappa') + \varepsilon \sum_{j=1}^{M} (A)_{ij} (Q_j' - Q_j)$$

+ $\varepsilon(C_i(Q_i') - C_i(Q_i)).$ (29)

Because $\sum_{i=1}^{M} Q_i = \sum_{i=1}^{M} Q_i' = Q$, summing over i for (29) gives $0 = \varepsilon(\kappa - \kappa') + \mathcal{O}(\varepsilon)$. Note that $\kappa, \kappa' \sim \mathcal{O}(\varepsilon^{-1})$, therefore in the limit as $\varepsilon \to 0^+$, we have that $\kappa - \kappa' = \mathcal{O}(1)$ and thus $Q_i - Q_i' = \mathcal{O}(\varepsilon)$. Substituting this back to (29) and noting that $C_i(\cdot)$ is continuously differentiable, we get

$$Q_{i} - Q'_{i} = \varepsilon(\kappa - \kappa') + \varepsilon \sum_{j=1}^{M} (A)_{ij} \mathcal{O}(\varepsilon) + \varepsilon C'_{i}(Q'_{i}) \mathcal{O}(\varepsilon)$$
$$= \varepsilon(\kappa - \kappa') + \mathcal{O}(\varepsilon^{2}), \tag{30}$$

where $C_i'(Q_i)$ is the derivative of $C_i(\cdot)$ at Q_i . Again, summing over i for (30) gives $0 = \varepsilon(\kappa - \kappa') + \mathcal{O}(\varepsilon^2)$, this further implies that $\kappa - \kappa' = \mathcal{O}(\varepsilon)$ and $Q_i - Q_i' = \mathcal{O}(\varepsilon^2)$. Applying this procedure repeatedly, by induction we know that $\kappa - \kappa' = \mathcal{O}(\varepsilon^L)$ and $Q_i - Q_i' = \mathcal{O}(\varepsilon^{L+1})$ for an arbitrary large L > 1 and hence we conclude that $\kappa = \kappa'$ and $Q_i = Q_i'$ for all $i = 1, \ldots, M$, which contradicts $\mathbf{v} \neq \mathbf{v}'$. So the nonlinear system (22) has a unique solution, and this completes the proof. \square

Furthermore, the first M entries of (27) implies that $Q_i = Q/M + \mathcal{O}(\varepsilon)$, $\forall i = 1, ..., M$, which becomes an interesting feature of the solution to (22): the value of Q_i for different i converges asymptotically to an equal value as $r_0 \to 0$ regardless of the charging function C_i and facility location x_i . This is summarized in the following proposition.

Proposition 5. *If the congestion function is linear within a bounded region* Ω *, and if the charging functions* C_i , $\forall I$,

and demand density function q(x) are bounded, the total facility flow throughputs in the equilibrium solution converge to $Q_1 = Q_2 = \cdots = Q_M$ as $r_0 \to 0$. The maximum difference between the set of flow values converges to zero at a rate of $-2\pi/\log r_0$.

Intuitively, this asymptotic result can be explained as follows. As $r_0 \rightarrow 0$, the congestion near the facilities increases dramatically, to an extent that it dominates the bounded service fee at each facility. Thus, customers could ignore the service fee but choose facilities based on congestion cost only. Because transportation cost would be dominated by that near the facility (where the total flux intensity approaches infinity), the actual travel distance becomes less important, and the number of customers choosing each facility tends to be equal regardless of the location of facilities. Proposition 5 thus implies that the size of facilities does have a significant impact on the PDE solution.

Based on the knowledge of total flux throughput Q_i , $\forall i$, the generalized cost $\phi(x)$ can be derived based on the boundary condition $\phi(\widetilde{x}_1) = C_1(Q_1)$ at facility 1. Note that $\phi(x)$ only differs from $u_1(x) + \cdots + u_M(x)$ by a constant. Therefore, we have

$$\phi(x) - \phi(\widetilde{x}_1) = \sum_{i=1}^{M} [u_i(x) - u_i(\widetilde{x}_1)].$$
 (31)

Substituting (18) into (31) yields

$$\phi(x) = C_1(Q_1) + \sum_{i=1}^{M} Q_i \left[N(x_i, \widetilde{x}_1) - N(x_i, x) \right]$$

$$+ \int_{\Omega} \left[N(x', x) - N(x', \widetilde{x}_1) \right] q(x') dx', \ \forall x.$$
 (32)

Moreover, if the weighted average of the Neumann function vanishes, that is, $\int_{\Omega} N(x',x)q(x) dx = 0$, $\forall x'$, the total cost can be further simplified, as stated in the following corollary.

Corollary 2. When Condition (20) holds and the Neumann function of region Ω is normalized with respect to q(x) (i.e., $\int_{\Omega} N(x',x)q(x) dx = 0$, $\forall x'$), the average customer cost under the continuous traffic equilibrium is given by

$$\bar{\phi} = C_1(Q_1) + \sum_{i=1}^{M} Q_i N(x_i, \tilde{x}_1).$$
 (33)

In the literature, continuous traffic equilibrium problems are generally solved by the finite element method (Yang and Wong 2000), and the average/total cost is estimated through numerical integration. However, Corollary 2 provides a much more efficient way to calculate the average/total cost; no discretization or integration over region Ω is needed. This property can be further used to simplify many difficult problems, for example, to optimize the location of service

facilities that minimize the system-wide cost. The optimal facility locations can now be determined by simply solving the following system of equations (either analytically or numerically):

$$\frac{\partial \bar{\phi}}{\partial x_i} = 0, \quad 1 \le i \le M. \tag{34}$$

In contrast, traditionally, the location optimization problem can only be solved by embedding the finite element method into other iterative solution algorithms, for example, see Ouyang et al. (2015), which normally bears prohibitive computation burdens. Moreover, Equation (33) implies that the average travel cost under traffic equilibrium is closely related to $-1/\log r_0$ (note the definition (10)) and if $r_0 \rightarrow 0^+$, the average cost would be infinitely large. So, numerical instability issues would arise when using numerical methods, which would yield large numerical errors and suboptimal designs. However, our analytical solution enables us to separate the singular term related to r_0 from other regular parts. Because we know the effect of $r_0 \rightarrow 0^+$ to the average cost, we can fully control the effect of r_0 and thus do not need to worry about the numerical fluctuations when solving the optimization problems.

4. Numerical Examples 4.1. Hypothetical Example

In this section, we present two hypothetical examples to illustrate the performance of the proposed solution framework. The first example is similar to the one in Ouyang et al. (2015), where the optimal location of multiple facilities is sought in a rectangle $\Omega = [0,a] \times [0,b]$. At location x, with coordinates $(x^{(1)}, x^{(2)})$, the demand density varies along the $x^{(1)}$ -axis, that is, $q(x) = \bar{q}(1 + \tau_q \cos(\pi x^{(1)}/a))$. The facility opening cost varies along the $x^{(2)}$ -axis, that is, $g(x) = \bar{g}(1 + \tau_g \cos(\pi x^{(2)}/b))$, and the facility service fee follows $C_i(Q) = 1 + \tau_c Q$, i = 1, 2, ..., M. Parameters $\tau_q \in$ [-1,1] and $\tau_g \in [-1,1]$ control the heterogeneity of q(x)and g(x) over Ω , respectively. For illustration purposes, we only solve the median-type facility problem (2), using the simple nonlinear optimization approach based on (34). Following Ouyang et al. (2015), we select $\bar{q} = 100$, $\bar{g} = 1$, $\tau_q =$ $\tau_g = 0.8, \tau_c = 0.01, B = 8, a = b = 1$ and the radius of facilities is $r_0 = 0.01$. The transportation cost function is selected to be the BPR-type (Bureau of Public Roads) function (Bureau of Public Roads 1964), that is, $c(x, \mathbf{f}(x)) = \alpha(x) + \beta(x) |\mathbf{f}(x)|^{\gamma(x)}$. In this example, we choose linear congestion, that is, $\alpha(x) \equiv 0, \beta(x) \equiv$

$$u_i(x) = -Q_i \left(N(x_i, x) - \frac{\tau_q a}{\pi^2 b} \cos\left(\frac{\pi x^{(1)}}{a}\right) \right), \tag{35}$$

where the Neumann function $N(x_i, x)$ is given by (14). Note that $|\Omega| = ab$, and hence $Q = \int_{\Omega} q(x) dx = \bar{q}ab$.

 $\gamma(x) \equiv 1$. As such, (18) can be specified as follows:

Therefore, for solving Q_i , (22) becomes the following: for $2 \le i \le M$,

$$C_{i}(Q_{i}) - C_{i-1}(Q_{i-1})$$

$$= \sum_{k=1}^{M} Q_{k} \left(N(x_{k}, \widetilde{x}_{i-1}) - N(x_{k}, \widetilde{x}_{i}) + \frac{\tau_{q} a}{\pi^{2} b} \left(\cos \left(\frac{\pi \widetilde{x}_{i-1}^{(1)}}{a} \right) - \cos \left(\frac{\pi \widetilde{x}_{i}^{(1)}}{a} \right) \right) \right), \quad (36)$$

and (32) is thus changed to

$$\phi(x) = C_1(Q_1) + \sum_{j=1}^{M} Q_i \left(N(x_i, \widetilde{x}_1) - \frac{\tau_q a}{\pi^2 b} \cos\left(\frac{\pi \widetilde{x}_1^{(1)}}{a}\right) \right) - \sum_{i=1}^{M} Q_i \left(N(x_i, x) - \frac{\tau_q a}{\pi^2 b} \cos\left(\frac{\pi x^{(1)}}{a}\right) \right).$$
(37)

Then average generalized cost is given by

$$\bar{\phi} = C_1(Q_1) + \frac{a\bar{q}}{b} \left(\frac{\tau_q^2}{2\pi^2} - \frac{\tau_q}{\pi^2} \cos\left(\frac{\pi \widetilde{x}_1^{(1)}}{a}\right) \right) + \sum_{i=1}^M Q_i \left(N(x_i, \widetilde{x}_1) - \frac{\tau_q a}{\pi^2 b} \cos\left(\frac{\pi x_i}{a}\right) \right).$$
(38)

For each set of locations x, the corresponding average cost ϕ can be evaluated by solving system (36) and evaluating (38), which takes only 0.01 seconds on average. As a comparison, using the finite element method with mesh generation (such as that in Ouyang et al. 2015), the average cost can hardly be obtained within 30 seconds on average. Using a nonlinear solver in MATLAB, the optimal location of facilities is obtained from solving (2) within 247 seconds (see Figure 3(a)). As a benchmark, the Lagrangian relaxation algorithm with embedded finite element method (Ouyang et al. 2015) requires 10.7 hours of computation time to solve an equivalent mixed-integer program (MIP) formulation with 25 candidate facility locations (i.e., the one in Ouyang et al. 2015), and yet leaving a 25% optimality gap (see Figure 3(b)). All computation experiments are implemented in a personal computer with 3.6 GHz CPU and 4 gigabytes memory. See "Unit square" scenario in Table 1 for a comparison.

The second example involves an irregular, nonconvex, and bounded service region as shown in Figure 4. Its boundary $\partial\Omega$ is described by the following parametric function in polar coordinates on the complex plane:

$$b(\theta)$$
= $(9\sin(\theta) + \cos^3(\theta) - 3\sin^2(\theta)\cos(\theta) - 4\sin(\theta)\cos(\theta))$
+ $i(-\sin^3(\theta) - 2\sin^2(\theta) + 2\cos^2(\theta) - 9\cos(\theta) + 3\sin(\theta)\cos^2(\theta))$,

The shape of Ω could represent an asymmetric twin city area. We will first apply the conformal mapping

 $0 \le \theta < 2\pi$.

scheme and the decomposition-based PDE solution method to obtain exact solution to the continuous traffic equilibrium problem for any given service facilities. To this end, the following conformal map transforms Ω into a unit disk D:

$$\zeta = h(x) =$$

$$-\frac{2j}{3} + \frac{(1-j\sqrt{3})}{6\sqrt[3]{2}} \left(3\sqrt{3}\sqrt{27x^2 + (324+32j)x + (-324+2,916j)}\right)$$
$$-27x + (-162-16j)^{\frac{1}{3}}$$
$$\left(\frac{4}{5} - 9j\right)(1+j\sqrt{3})$$

$$-\frac{\left(\frac{4}{3}-9j\right)(1+j\sqrt{3})}{2^{2/3}}\left(3\sqrt{3}\sqrt{27x^2+(324+32j)x+(-324+2,916j)}\right)$$
$$-27x+(-162-16j)^{-\frac{1}{3}}.$$
 (40)

The inverse map is simple: $x = h^{-1}(\zeta) = \zeta^3 + 2j\zeta^2 - 9j\zeta$. Note that $x = b(\theta)$ and $\zeta = \exp(j\theta)$ are the corresponding points on $\partial\Omega$ and ∂D , respectively.

Basic calculus shows that the normal vector as a function of $\theta \in [0, 2\pi)$ is

$$\mathbf{n}_{x}(\theta) = \left(\frac{-9\sin(\theta) + 4\sin(2\theta) - 3\cos(3\theta)}{\sqrt{24\sin(\theta) - 54\sin(2\theta) - 72\cos(\theta) + 106}}, \frac{-3\sin(3\theta) + 9\cos(\theta) - 4\cos(2\theta)}{\sqrt{24\sin(\theta) - 54\sin(2\theta) - 72\cos(\theta) + 106}}\right). \tag{41}$$

The area of Ω is as follows:

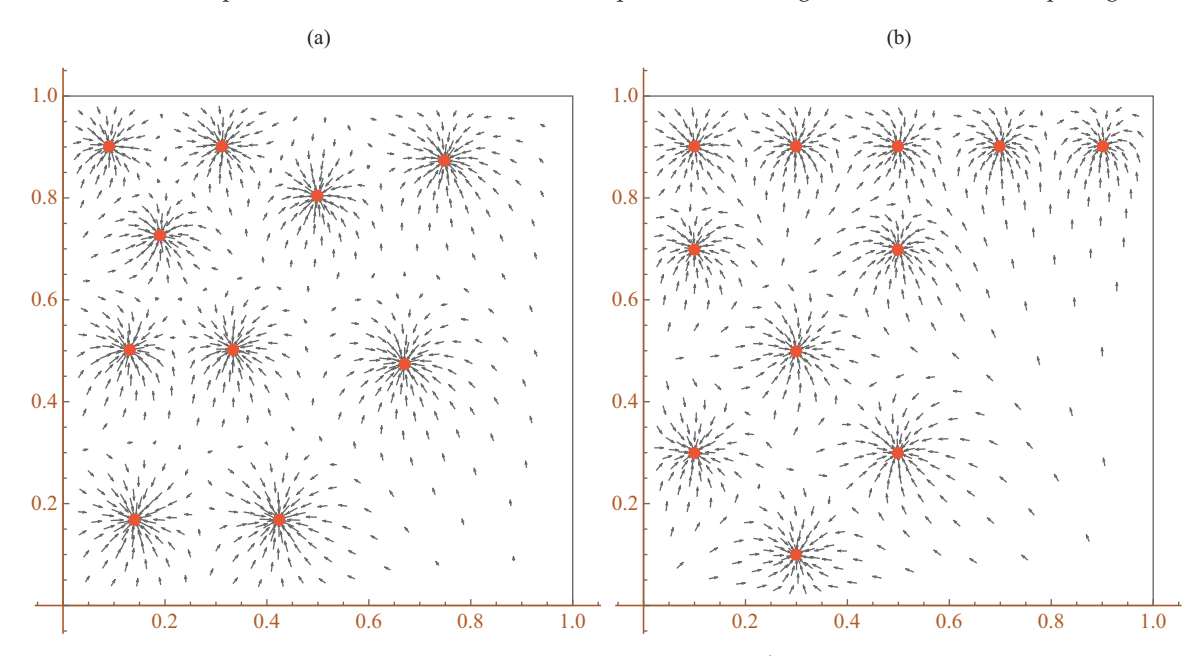
$$|\Omega| = \int_0^{2\pi} \int_0^1 |(h^{-1})'(re^{i\theta})|^2 r \, dr d\theta = 92\pi.$$
 (42)

Hence, (16) can be specified by means of (41) and (42), where $\mathbf{n}_{h^{-1}(e^{j\theta})} = \mathbf{n}_x(\theta)$. As such, the Neumann function of Ω can be expressed analytically and thus (2a) can be specifically derived.

Suppose now that the optimal locations of multiple facilities are sought in Ω to minimize the average cost per unit demand. The demand is homogenous, that is, $q(x) \equiv \bar{q}$, but the facility opening cost varies with the distance to the origin (0, 0), specifically, $g(x) = \bar{g}(1 + \tau_g \cos(\pi |h(x)|))$. The facility service fee still follows $C_i(Q) = 1 + \tau_c Q$, i = 1, 2, ..., M. We choose $\bar{q} = \bar{g} = 1$, $\tau_g = 0.8$, $\tau_c = 0.01$, $\mathcal{B} = 4$, and $r_0 = 0.3$, and then solve (2) via a nonlinear solver.

For each set of locations x, the corresponding average $\cos t \bar{\phi}$ can be evaluated in 6.9 seconds on average whereas the finite element method with mesh generation takes 30 seconds on average. The computation burden of the proposed method is heavier for this case than that for the unit square case (despite their similar problem size), because the Neumann function obtained by (16) for Ω is no longer normalized—in such cases, a numerical integration must be computed for (32).⁸ The optimal solution, found within 59 minutes of computation time, is shown in Figure 5(a),

Figure 3. (Color online) Optimal Locations of Facilities in Unit Square with Heterogeneous Demand and Opening Cost



Note. (a) Optimal solution using nonlinear solver based on (38). Minimum average cost $\bar{\phi}^* = 4.87$. (b) Optimal solution using Lagrangian relaxation algorithm. Minimum average cost $\bar{\phi}^* = 5.03$.

with a minimum average cost of $\bar{\phi}^* = 9.92$. Interestingly, note that none of the facilities is distributed around the center of the region, where facility construction cost is relatively high and traffic flux is likely to concentrate. In contrast, the Lagrangian relaxation algorithm with embedded finite element method subroutine (Ouyang et al. 2015) takes 11.1 hours to find a solution to the corresponding MIP formulation (with 25 candidate locations), leaving a 30% optimality gap. The best average cost is 10.99, about 10.8% higher than that from the nonlinear optimization approach. This comparison demonstrates the superiority of the proposed method in terms of solution quality and computational performance, which is expected to be even more prominent for larger problem instances. See "Irregular, nonconvex" scenario in Table 1 for a comparison.

4.2. Empirical Example

The examples presented in Section 4.1 used hypothetical data to show how the closed-form analytical PDE solution (in contrast to numerical solutions from traditional finite element methods) helps facilitate facility

location design by achieving a shorter computation time and a superior convergence process. This subsection further demonstrates the applicability of the closed-form formulas and the facility location design framework through a full-scale example. In so doing, we plan the location of metro station entrances in the Beijing Railway Station North Square, China. The purpose of this example is to show (i) how traffic congestion and equilibrium can be captured by our PDE model with reasonable fidelity, and (ii) how the proposed facility location design model could be used to improve pedestrian traffic facilities.

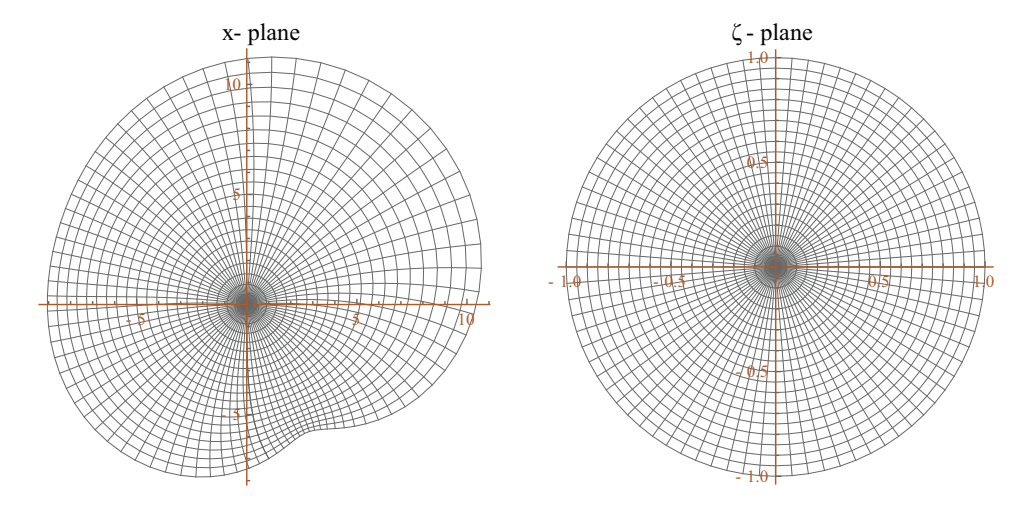
The Beijing Railway Station is a major intercity railway station in Beijing, serving extremely high pedestrian traffic in peak seasons (up to 175 thousand daily; see Yi 2020). The North Square of the station, surrounded by nearly rectangular street grids, is the key hub for passengers to transfer between the intercity railway system and city transportation systems. A large majority of these transfer passengers take the metro, and currently the metro station's entrances are located on the far side of the North Square in Figure 6(a).

Table 1. Comparison of the Numerical Results

Scenario	Computation time	for average cost	Computation time f	Optimal cost		
	CF	FE	CF + NS	FE + LR	CF + NS	FE + LR
Unit square Irregular, nonconvex	0.01 sec 6.9 sec	30 sec 30 sec	247 sec 59 min	10.7 hr 11.1 hr	4.87 9.92	5.03 10.99

Note. CF, closed-form formulas; FE, finite element method; LR, Lagrangian relaxation; NS, MATLAB nonlinear solver.

Figure 4. (Color online) Region Ω (Left) and Unit Disk D (Right) Based on Mapping Function (40)



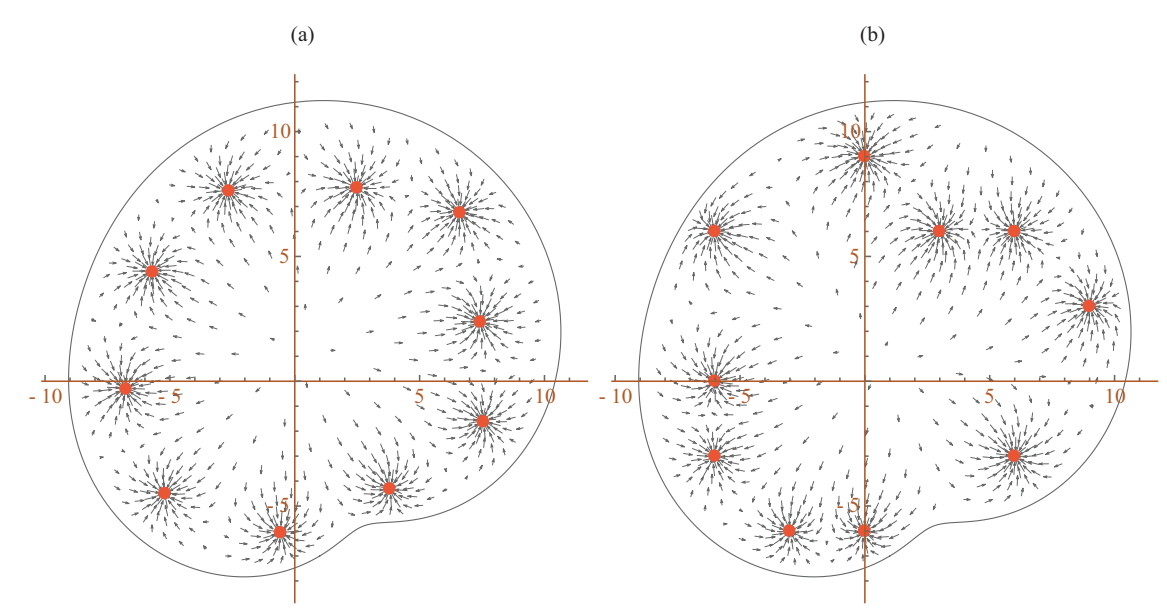
The North Square has been extremely congested during most of the day; see Figure 6(b) for a photo of the typical crowd on the Square. The city's government agencies have been very concerned about the pedestrian traffic capacity of this transfer hub in case of major public events, especially as they prepare for the upcoming 2022 Beijing Winter Olympics.

In this illustrative example, we first evaluate the pedestrian traffic efficiency, measured by pedestrian travel time under congestion, under the current North Square layout. We approximate the North Square by a rectangular domain that can be further partitioned into multiple subdomains, each of which represents a surrounding demand area (e.g., railway entrance, ticket office, shopping mall, hotel, parking lot). The shape and dimension of each demand area (measured

in feet (ft)) are shown in Figure 7(a), and a coordinate system is set up with its origin at the lower-left corner of the Square. The two current metro station entrances are located at $x_1 = (350, 150), x_2 = (350, 775)$. To stay focused, we only consider the peak-hour steady-state pedestrian travel demand between the metro entrances and these surrounding demand areas, and further model the traffic to be originating from those demand areas and destined toward either of the metro station entrances. The demand density values q(x) (measured in person per square foot per hour) are assumed to vary across demand areas, as marked in Figure 7(a). This setup generates about 85,000 pedestrians per hour in total.

Because the domain $\Omega = [0,400]$ ft $\times [0,925]$ ft is rectangular, (14) can be used to derive the Neumann

Figure 5. (Color online) Facility Location Design in an Irregular Ω



Note. Solution from (a) nonlinear optimization and (b) Lagrangian relaxation.

Figure 6. (Color online) Beijing Railway Station North Square





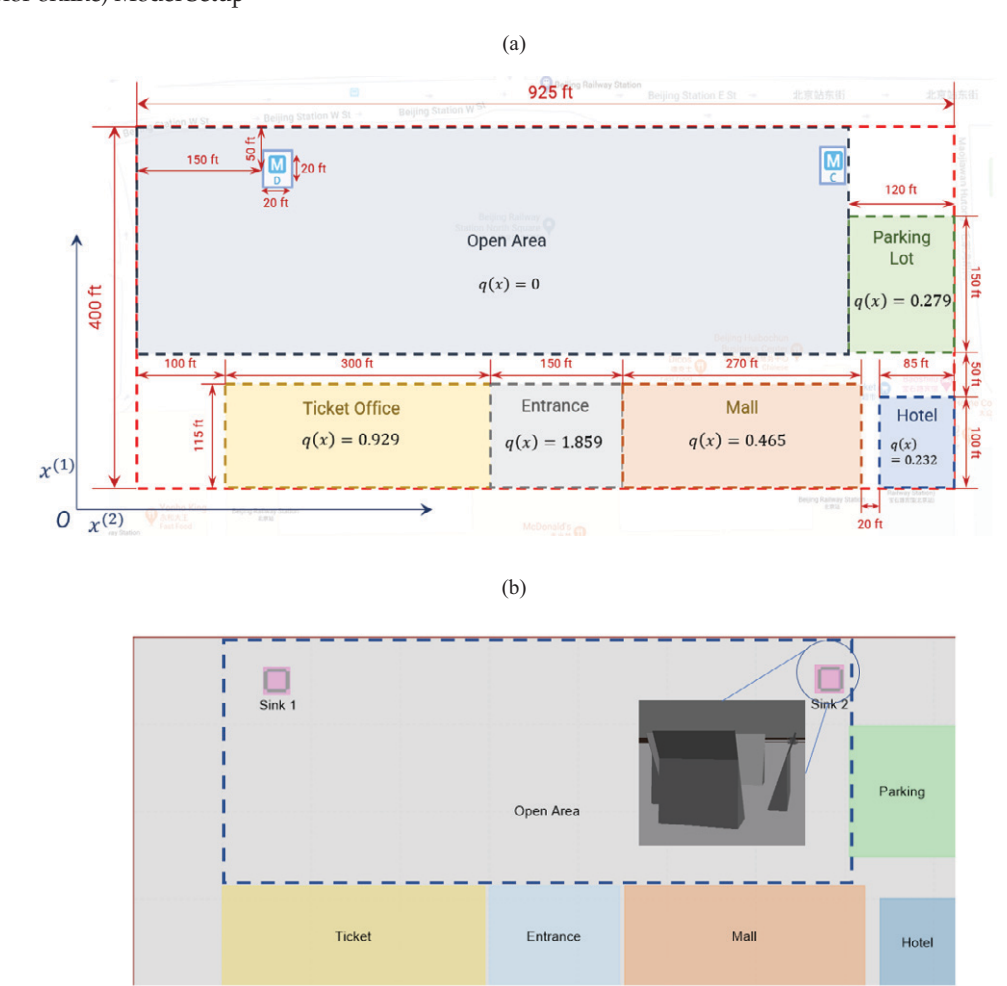
Source. Reuters 2018 (b) Note. (a) Map and (b) the crowd.

function N(x',x). Therefore, we choose the same linear congestion function as the ones in Section 4.1 (with parameters $\alpha=0,\beta=2.26$, and $\gamma=1$), and assume that it is location independent within Ω . We further set the radius of two circular metro station entrances (approximating a square) to be $r_0=20$ ft. As such, we can substitute q(x) into (18) and (22) to analytically estimate the average generalized cost $\bar{\phi}$ for the given metro station entrances.

Meanwhile, to verify our analytical PDE model, we use a state-of-art simulation package, PTV Viswalk (PTV

2014) as a tool for benchmarking. PTV Viswalk is a discrete-event agent-based simulator that uses the social force model (Helbing and Molnar 1995) to mimic individual pedestrian's motion behavior. It captures pedestrians' desire to reach their destinations, the mutual influences among pedestrians, as well as all surrounding objects. This simulation package has been intensively calibrated and widely used for reproducing pedestrian traffic in complex, crowded situations (such as railway stations and stadiums); see Peiponen (2017), Wibowo and Fadilah (2018), and Martén and Henningsson (2014) for examples.

Figure 7. (Color online) Model Setup



Note. (a) Subdomain partition and (b) simulation model setup in Viswalk.

The full-scale simulation setup in Viswalk is fairly straightforward, as shown in Figure 7(b). For modeling convenience, we set up two square metro entrances, and use identical ramps to approximate the gates of each entrance. These ramps are all connected to a common destination (i.e., the metro system). Each pedestrian chooses its fastest path to reach the common destination via any of the ramps.

Viswalk uses a range of agent-based model parameters (e.g., desired speed, and safety distance between adjacent pedestrians) to describe the behavior and interactions of pedestrians. We select the parameter combinations that could best fit with the traffic flux pattern from the PDE model under the current metro entrance design, and these values are shown in Table 2. Interested readers are referred to Viswalk's

manual (PTV 2014) for detailed interpretation of these parameters, so we only give a brief explanation in the following. Here, we set a very large desired speed v_0 to capture the pedestrians' rush toward their destinations. Parameters A_{si} (ft/second (s)²), B_{si} (ft), A_{sm} (ft/ s^2), B_{sm} (ft), and r (ft) jointly control the strength of repulsive forces between neighboring pedestrians, and we use rather large values such that the pedestrians are sensitive to crowds. Parameter τ takes a large value to show that the pedestrians are willing to take detours to avoid congested areas. Other parameters, such as VD, react to n, and noise, have secondary effects and take their default values from the user manual. To avoid local gridlocks near the entrance ramps (i.e., similar to singular flux in the PDE model), we surround the ramps with a subdomain, approximately five feet wider

Table 2. Pedestrian Behavior Parameters in Viswalk

Parameter	v_0	$A_{\rm si}$	B_{si}	$A_{\rm sm}$	$B_{\rm sm}$	λ	τ	VD	r	React to n	Noise
Value	16 mph	4.0	12.0	4.0	12.0	1.0	3.0	3.0	30	8	1.2

than the ramps, and assign $\tau = 0.05$ and $v_0 = 24$ miles per hour (mph). Each simulation will run for a total of 600 seconds, and the pedestrians' statistics are collected after a warm-up period of 200 seconds (when the traffic becomes almost steady).

The flux vector fields from the analytical PDE solution and the Viswalk simulations are plotted in Figure 8, (a) and (b), respectively. It can be observed that the flux patterns from the two models are largely similar, whereas that from the PDE model is more diffusive and smooth, possibly as a result of the fluidlike continuous flow description. In contrast, the flux distribution from the Viswalk simulation has sharper boundaries between void and nonvoid areas, possibly because it is consolidated from discrete pedestrian agent trajectories. Despite that, both figures show curvy travel paths around the sinks, indicating that the pedestrians are naturally pushed away from each other, and they have to detour away from their shortest paths. As a result, in both figures, traffic uses even the farther side of the sinks to avoid congestion, and fills up

almost the entire open space. In less congested areas, the flux vectors are rather laminar. These obvious similarities between the vector fields, particularly those at the congested regions, demonstrate that the pedestrians' congestion-avoiding behavior is fairly well represented by the analytical model.

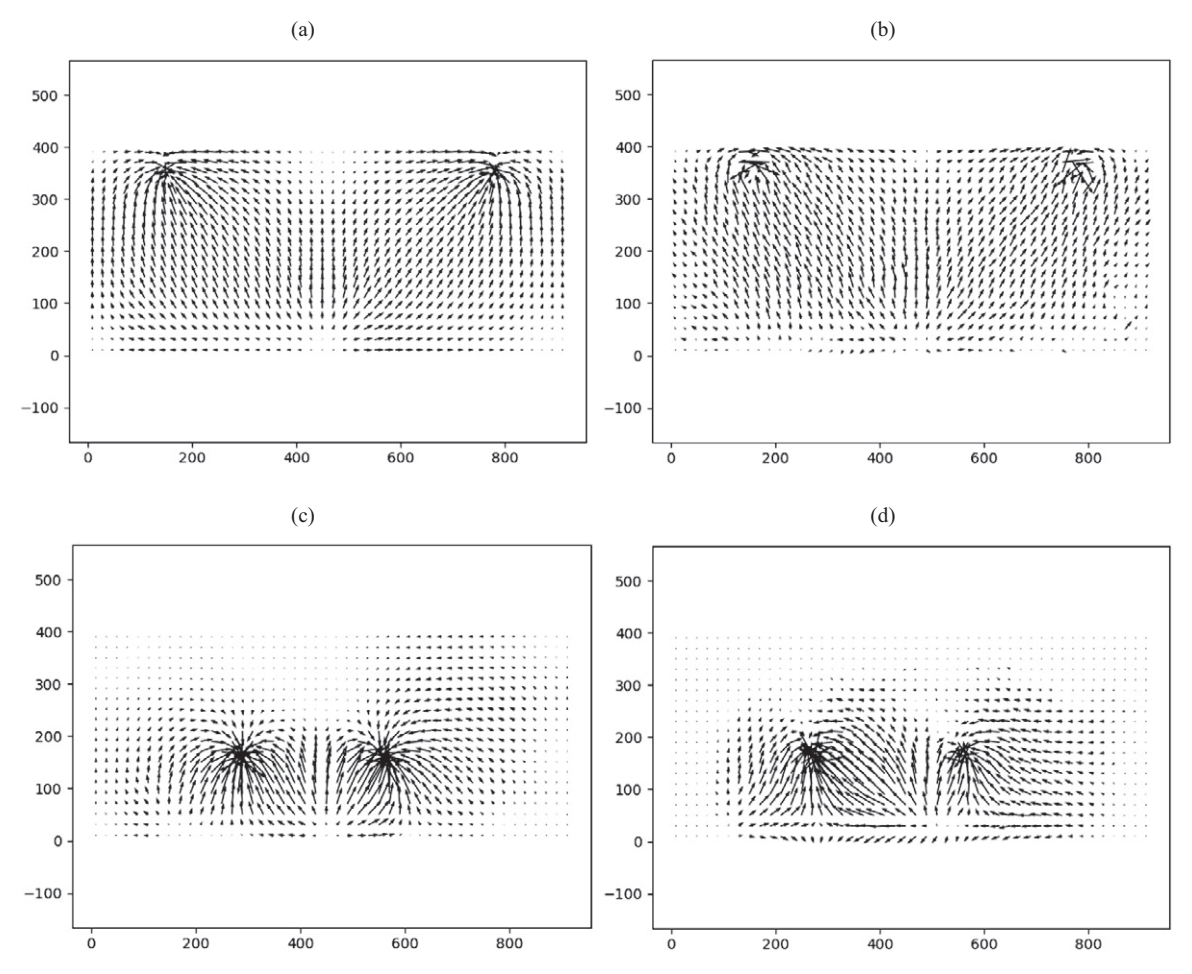
The relative error between the analytical flux vector field $\mathbf{f}(x)$ and the simulated flux vector field, denoted $\mathbf{f}'(x)$, is measured⁹ over a discrete set of sample points, X, as follows:

$$E(\mathbf{f}, \mathbf{f}' \mid \alpha, \beta, \gamma) = \frac{1}{|X|} \sum_{x \in X} \frac{\|\mathbf{f}(x) - \mathbf{f}'(x)\|}{\|\mathbf{f}(x)\|},$$

where $X = \{x \mid x \in \Omega_{eval}, |x - x_i| \ge 15 \text{ ft } \forall i, ||\mathbf{f}(x)|| \ge 0.0001\}$, and Ω_{eval} is the open area marked by the dashed box in Figure 7(b). The value of $E(\mathbf{f}, \mathbf{f}')$ for Figure 8, (a) and (b) is 16.7%.

The statistics of traffic performance for both the analytical PDE solution and Viswalk simulation are reported in the first column of Table 3. Comparing to

Figure 8. (Color online) Flux Vector Fields of the PDE Solution and Viswalk Simulation



Note. (a) Current layout, PDE; (b) current layout, Viswalk; (c) optimized layout, PDE; (d) optimized layout, Viswalk.

Table 3. Comparison of Pedestrian Traffic Statistics Under Different Designs

Statistics	Current $x_1 : (350, 150), x_2 : (350, 775)$		1	imized s), x ₂ : (150,554)	Optimized without congestion $x_1: (150,389), x_2: (150,769)$		
	PDE	Viswalk	PDE	Viswalk	PDE		
Average travel cost	32.89	38.46	19.77	26.15	22.16		
Average speed	3.12	2.87	6.76	5.03	3.74		
Q_1/Q_2	99.1%	98.4%	93.8%	104.8%	170%		

the simulation result, the average travel cost is within 20% of those by the PDE, and the prediction of pedestrians' facility choice (i.e., indicated by Q_1/Q_2) is also in good accordance.

Now we are ready to embed the PDE solution into the location optimization model for the North Square. The goal is to redesign the locations of the two entrances such that the pedestrian congestion during peak hours can be mitigated. To simplify the process, we choose to only relocate the two existing entrances without adding new ones. Hence, the facility set-up cost is constant and hence can be ignored in the objective function. Similar to the examples in Section 4.1, we use MATLAB's nonlinear solver. With direct evaluation of the analytical PDE solution, the optimal locations can be found within three seconds as the following: $x_1 = (150, 288), x_2 = (150, 554)$. The corresponding pedestrian flux vector field is plotted in Figure 8(c), and the traffic performance statistics are shown in the second column of Table 3. For comparison, we again use Viswalk to simulate the pedestrian traffic under the optimal design, and this time we directly use the same setup and parameter values as those in Table 2. The corresponding flux vector field and performance statistics are given in Figure 8(d) and Table 3 as well. The flux vector fields now have a slightly larger difference with $E(\mathbf{f}, \mathbf{f}') = 34.4\%$, but the general flux pattern and the service performance statistics are reasonably similar. Notably, both models have yielded almost equal throughputs at the two metro station entrances, illustrating how the pedestrians' mesolevel route choices at equilibrium are driven by congestion. Considering the drastically different assumptions underlying the analytical and simulation models, our results show reasonably good performance of the analytical solution in (i) predicting pedestrian flow under equilibrium, and (ii) estimating the potential saving from optimized facility location design. After relocating the two metro station entrances, the PDE model predicts that the average travel cost is reduced by 39.6%. The simulation result shows a reduction of 32%, which is fairly close considering the difference in nature of these two models.

Finally, it is interesting to check the importance of considering the impacts of traffic congestion in the

process of optimal location design. In so doing, we design the metro entrance locations without considering any congestion, and use the same MATLAB nonlinear solver to solve the same problem, but with $\alpha > 0, \beta = \gamma = 0$ (i.e., no congestion impact exists, and also note that the exact value of α does not affect the optimal locations because the total cost is proportional to α as long as it is positive). This problem is equivalent to a typical two-median problem (Tansel et al. 1983). The optimal locations obtained in this setting are found to be $x_1 = (150, 389), x_2 = (150, 769)$. Then, we evaluate the traffic service performance under this new location design when congestion exists (with the same congestion parameters in the PDE model), The average travel cost with congestion is 22.16, which is around 12.1% higher than the minimal cost (19.77) under the optimal design. This simple comparison illustrates why it is important to consider congestion and traffic equilibrium in facility location design.

5. Conclusion

This paper proposed a decomposition method for solving a class of PDEs that describe user equilibrium (UE) traffic behavior in a continuous two-dimensional space. This class of problems has significance in a range of application contexts. We have shown that under certain conditions, the solution to the PDEs can be obtained by solving multiple Neumann problems in a bounded region. One key advantage of this approach is that closed-form solution to the Neumann problem is readily available for some specific cases, for example, when the demand region forms a circular disk, a rectangle, or an equilateral triangle. When the demand region takes an arbitrary shape, we further propose a conformal mapping scheme that helps transform the demand region to obtain exact analytical PDE solutions. Moreover, several properties of the analytical solutions are discussed, which leads to formulas for calculating the average system cost as well as the total flow throughput at each facility. In contrast to traditional PDE solution approaches (such as the finite element method), the proposed methodology not only sheds light on the properties of continuous traffic equilibrium but also holds the promise to reduce the computational burden. Computational experiments demonstrate significant savings on

computation time and accuracy associated with solving for continuous UE and seeking optimal service facility locations.

Future research can be conducted in many directions. In this paper, all the analytical solutions are derived based on assumption (4) on the travel cost function $c(x, \mathbf{f})$. However, in some more general cases where (4) is violated, the problem can still be solved approximately. In future studies, approximated methods building upon the analytical results proposed in this paper can be developed to efficiently find solutions where the travel costs are described by general nonlinear functions (e.g., those derived from realistic traffic fundamental diagrams). Along this line, the model can be improved by replacing the flow-based cost formulation with density-based counterparts to better represent realistic traffic behavior in heavy congestion. In addition, in this paper, disruption risks of facilities are not considered during the optimization. Addressing reliable facility location design under continuous traffic equilibrium and probabilistic facility disruption risks will be another challenging topic.

Acknowledgments

The majority of this research was conducted while Z. Wang was a graduate student at the University of Illinois. The authors thank Professor Richard S. Laugesen (University of Illinois Urbana-Champaign) for providing insightful suggestions on the Neumann functions, and Yiduo Huang (visiting student from Tsinghua University) for implementing the finite element method (as the benchmark) for the hypothetical examples in Section 4.1. They thank Professor Hai Yang (Hong Kong University of Science and Technology) for providing helpful comments on an earlier version of the paper. They also thank the area editor, associate editors, and two anonymous referees for many constructive comments that helped to greatly improve the paper.

Endnotes

- ¹ The trajectories actually mark the pedestrians' head locations, which include minor wiggles due to lateral body movements while walking.
- ² Formulation (1) can be used to describe different types of equilibria, for example, user equilibrium (Wardrop 1952) when customers are completely rational and interested in their own costs. In applications that involve central control (e.g., commercial drone operations), traffic may be better represented by a system optimal flux pattern (Wardrop 1952). In such cases, we can still use the same formulation (1) as long as the link cost function is properly defined to include the marginal externality, that is, instead of using the actual cost to each traveler, $c(x, \mathbf{f}(x))$, we can use $c(x, \mathbf{f}(x)) + |\mathbf{f}(x)| \cdot \frac{\partial}{\partial f(x)} c(x, \mathbf{f}(x))$. This is explained in more detail in Ouyang et al. (2015). In emergency situations, pedestrian behavior may be irrational (e.g., by exhibiting herd behavior). Further studies would be needed for such cases.
- ³ The real-world congestion cost function can take many forms, and linearity might be reasonable when traffic delay is considerably

- larger than free flow travel time (e.g., in heavy traffic). See figure 10 in Steffen and Seyfried (2010). Note how the scattered points roughly form an inverse curve. So after proper regression, the travel time can be approximately linear of density/flux.
- ⁴ If Condition (4) is violated, the problem can still be solved to obtain an approximate solution for further refinement (e.g., as the initial solution for a nonlinear finite element method). We leave this topic for future research.
- ⁵ We shall note that the solution u(x) is not unique, but any two solutions differ by a constant (see theorem 3-2 in Guenther and Lee 1996). By removing the last term \bar{u} , we could obtain a normalized solution to the Neumann problem satisfying $\iint_{\Omega} u(x,x') dx dx' = 0$.
- ⁶ The converse, that is, (1a) and (1e) implying (3), is not necessarily true. However, this does not affect the correctness of Proposition 1, because (8) does solve the original PDEs (1) asymptotically as $r_0 \to 0^+$.
- ⁷ The BPR-type function is widely used in the transportation planning literature but it does not capture the phenomenon that a higher speed may be associated with a higher flow in very congested traffic. It may be more appropriate to explore other variants of the cost function (e.g., those obtained from the traffic fundamental diagram, or those relating speed to traffic density). Those options will be left for future research.
- ⁸ We use a simple algorithm to estimate the numerical integration in this nonconvex region. First, we use meshgrid to generate a grid of sampled points and get the corresponding values of the integrand. The integrand returns NaN for points lying outside the region. Then we use nanmean multiplied by the area of the region to obtain the value of the integral. The extra computational complexity added to each optimization step is $\mathcal{O}(K)$, where K is the size of the grid. Note that the evaluation of the integrand using closed-form formula only takes $\mathcal{O}(1)$ computation time.
- ⁹ In Viswalk, local traffic characteristics, including average density and velocity, can be evaluated using local screening sections. The product of the two, measured over an array of sections, yields the flux.

References

- Abdelghany A, Abdelghany K, Mahmassani H, Al-Zahrani A (2012) Dynamic simulation assignment model for pedestrian movements in crowded networks. *Transportation Res. Record J. Transportation Res. Board* 2316:95–105.
- Ahlfors LV (1966) Complex Analysis (McGraw-Hill, New York).
- An S, Cui N, Bai Y, Xie W, Chen M, Ouyang Y (2015) Reliable facility location design under service disruption, en-route congestion and in-facility queuing. *Transportation Res. Part E Logist. Transportation Rev.* 82:199–216.
- Baggaley K (2017) Air taxis are about to take off. This one just did. NBC News (October 5), https://www.nbcnews.com/mach/science/air-taxis-are-about-take-one-just-did-ncna807416.
- Bai Y, Ouyang Y, Pang J (2016) Enhanced models and improved solution for competitive biofuel supply chain design under land use constraints. Eur. J. Oper. Res. 249(1):281–297.
- Bai Y, Hwang T, Kang S, Ouyang Y (2011) Biofuel refinery location and supply chain planning under traffic congestion. *Transportation Res. Part B Methodological* 45(1):162–175.
- BBC News (2015) Shanghai new year crush kills 36. BBC (January 1), https://www.bbc.com/news/world-asia-china-30646918.
- Bureau of Public Roads (1964) *Traffic Assignment Manual*, U.S. Dept. of Commerce, Urban Planning Division, Washington, DC.
- Carlsson JG, Jia F (2013) Euclidean hub-and-spoke networks. *Oper. Res.* 61(6):1360–1382.
- Carlsson JG, Jia F (2015) Continuous facility location with backbone network costs. Transportation Sci. 49(3):433–451.

- Chow D (2018) Uber just unveiled a prototype of its futuristic air taxi. NBC News (May 9), https://www.nbcnews.com/mach/science/uber-just-unveiled-prototype-its-futuristic-air-taxi-ncna872771.
- Du Y, Wong S, Sun L (2016) A multi-commodity discrete/ continuum model for a traffic equilibrium system. *Transport*metrica A Transportation Sci. 12(3):249–271.
- Feng L, Miller-Hooks E (2014) A network optimization-based approach for crowd management in large public gatherings. *Transportation Res. Part C Emerging Tech.* 42:182–199.
- Gao Z, Qu Y, Li X, Long J, Huang HJ (2014) Simulating the dynamic escape process in large public places. *Oper. Res.* 62(6):1344–1357.
- Gariel M, Srivastava AN, Feron E (2011) Trajectory clustering and an application to airspace monitoring. *IEEE Trans. Intelligent Transportation Systems.* 12(4):1511–1524.
- Gladstone R (2015) Death toll from Hajj stampede reaches 2,411 in new estimate. *New York Times* (December 10), https://www.nytimes.com/2015/12/11/world/middleeast/death-toll-from-hajj-stampede.html.
- Guenther R, Lee J (1996) Partial Differential Equations of Mathematical Physics and Integral Equations, Dover Books on Mathematics (Dover Publications, Mineola, NY).
- Hajibabai L, Bai Y, Ouyang Y (2014) Joint optimization of freight facility location and pavement infrastructure rehabilitation under network traffic equilibrium. *Transportation Res. Part B Methodological* 63:38–52.
- Hajibabai L, Ouyang Y (2013) Integrated planning of supply chain networks and multimodal transportation infrastructure expansion: Model development and application to the biofuel industry. Comput. Aided Civil Infrastructure Engrg. 28(4):247–259.
- Helbing D, Buzna L, Johansson A, Werner T (2005) Self-organized pedestrian crowd dynamics: Experiments, simulations, and design solutions. *Transportation Sci.* 39(1):1–24.
- Helbing D, Molnar P (1995) Social force model for pedestrian dynamics. *Physical Rev. E.* 51(5):4282–4286.
- Henrici P (1993) Applied and Computational Complex Analysis, Discrete Fourier Analysis, Cauchy Integrals, Construction of Conformal Maps, Univalent Functions, vol. 3. (John Wiley & Sons, Hoboken, NJ).
- Ho H, Wong S (2005) A Levenberg–Marquardt iterative solver for leastsquares problems. Comm. Numer. Methods Engrg. 21(6):327–335.
- Ho H, Wong S (2006) Two-dimensional continuum modeling approach to transportation problems. J. Transportation Systems Engrg. Inform. Tech. 6(6):53–68.
- Ho H, Wong S, Loo B (2003) A continuous traffic equilibrium model with multiple user classes. *J. Eastern Asia Soc. Transportation Stud.* 5:2831–2845.
- Hoogendoorn SP, Daamen W (2005) Pedestrian behavior at bottlenecks. *Transportation Sci.* 39(2):147–159.
- Jiang L, Mahmassani H, Zhang K (2011) Congestion pricing, heterogeneous users, and travel time reliability: Multicriterion dynamic user equilibrium model and efficient implementation for large-scale networks. *Transportation Res. Record J. Transportation Res. Board* 2254(1)58–67.
- Kolokolnikov T, Titcombe MS, Ward MJ (2005) Optimizing the fundamental Neumann eigenvalue for the Laplacian in a domain with small traps. *Eur. J. Appl. Math.* 16(02):161–200.
- Konur D, Geunes J (2011) Analysis of traffic congestion costs in a competitive supply chain. *Transportation Res. Part E Logist. Transportation Rev.* 47(1):1–17.
- Konur D, Geunes J (2012) Competitive multi-facility location games with non-identical firms and convex traffic congestion costs. *Transportation Res. Part E Logist. Transportation Rev.* 48(1):373–385.
- Li AC, Nozick L, Xu N, Davidson R (2012) Shelter location and transportation planning under hurricane conditions. *Transportation Res. Part E Logist. Transportation Rev.* 48(4):715–729.
- Long J, Szeto WY (2019) Link-based system optimum dynamic traffic assignment problems in general networks. *Oper. Res.* 67(1): 167–182.

- Mahmassani HS, Chen P (1993) An investigation of the reliability of real-time information for route choice decisions in a congested traffic system. *Transportation* 20(2):157–178.
- Marsden JE, Tromba A (2003) Vector Calculus (Macmillan, New York).
- Martén JB, Henningsson J (2014) Verification and validation of Viswalk for building evacuation modelling. Master thesis, Department of Fire Safety Engineering, Lund University, Sweden.
- McCartin BJ (2011) Laplacian Eigenstructure of the Equilateral Triangle (Hikari, Limited, Rousse, Bulgaria).
- Ouyang Y, Wang Z, Yang H (2015) Facility location design under continuous traffic equilibrium. *Transportation Res. Part B Methodological* 81:18–33.
- Papamichael N, Stylianopoulos N (2010) Numerical Conformal Mapping: Domain Decomposition and the Mapping of Quadrilaterals (World Scientific, Hackensack, NJ).
- Peeta S, Mahmassani HS (1995) System optimal and user equilibrium time-dependent traffic assignment in congested networks. Ann. Oper. Res. 60(1):81–113.
- Peiponen J (2017) Pedestrian assessment of a new football stadium in Zürich, Switzerland. Unpublished bachelor's thesis, Hämeen ammattikorkeakoulu.
- PTV (2014) Ptv Vissim 7 User Manual (Karlsruhe, Germany).
- Reisinger D (2018) Check out the Uber air flying car that will transport passengers of the future. *Fortune* (May 8), https://fortune.com/2018/05/08/uber-air-flying-car-drone-video/.
- Reuters (2018) Chinese spend more on restaurants, movies, travel during new year holiday. Reuters (February 21), https://www.reuters.com/article/us-china-economy-consumer-idUSKCN1G51VC.
- Roach GF (1982) *Green's Functions*, vol. 239 (Cambridge University Press, Cambridge, UK).
- She R, Ouyang Y (2021) Efficiency of UAV-based last-mile delivery under congestion in low-altitude air. *Transportation Res. Part C Emerging Tech.* 122:102878–102891.
- Sherali HD, Carter TB, Hobeika AG (1991) A location-allocation model and algorithm for evacuation planning under hurricane/flood conditions. *Transportation Res. Part B Methodological* 25(6):439–452.
- Steffen B, Seyfried A (2010) Methods for measuring pedestrian density, flow, speed and direction with minimal scatter. *Physica A*. 389(9):1902–1910.
- Tansel BC, Francis RL, Lowe TJ (1983) State of the art-location on networks: A survey. Part I: The *p*-center and *p*-median problems. *Management Sci.* 29(4):482–497.
- Toh M, Ostrower J (2018) People are now flying around in autonomous drones. CNN Business (February 8), https://money.cnn.com/2018/02/08/technology/ehang-self-flying-drone/index.html.
- Wang Z (2018) Planning service facilities and infrastructures under continuous traffic equilibrium. PhD dissertation, University of Illinois at Urbana-Champaign.
- Wang Z, Xie S, Ouyang Y (2021) Planning facility location in a continuous space under congestion and disruption risks. Working paper, University of Illinois at Urbana-Champaign.
- Wardrop JG (1952) Road paper. Some theoretical aspects of road traffic research. *Proc. Institution Civil Engineers* 1(3):325–362.
- Wibowo SS, Fadilah SR (2018) Queuing analysis using Viswalk for check-in counter: Case study of Lombok Praya international airport. MATEC Web Conf. 181:2006–2018.
- Williamson RE, Trotter HF (1996) Multivariable Mathematics (Prentice Hall, Upper Saddle River, NJ).
- Wong S, Sun S (2001) A combined distribution and assignment model for continuous facility location problem. *Ann. Regional Sci.* 35(2):267–281.
- Wong SC, Zhou C, Lo HK, Yang H (2004) Improved solution algorithm for multicommodity continuous distribution and assignment model. J. Urban Planning Development 130(1): 14–23.

- Yang H (1996) A spatial price equilibrium model with congestion effects. Ann. Regional Sci. 30(4):359–371.
- Yang H, Wong S (2000) A continuous equilibrium model for estimating market areas of competitive facilities with elastic demand and market externality. *Transportation Sci.* 34(2):216–227.
- Yang H, Yagar S, Iida Y (1994) Traffic assignment in a congested discrete/continuous transportation system. *Transportation Res.* Part B Methodological 28(2):161–174.
- Yi H (2020) Beijing's five major railway stations deliver 600,000 passengers a day. *Beijing Youth Daily* (January 23), https://news.sina.cn/gn/2020-01-23/detail-iihnzahk5884470.d.html.
- Zhang XS, Li W, Ouyang Y (2021) Paved guideway topology optimization for pedestrian traffic under Nash equilibrium. Structural Multidisciplinary Optim. 63(3):1405–1426.

Zhaodong Wang is a senior research engineer at Netflix Inc. He received his PhD in civil engineering from the University of Illinois at Urbana-Champaign.

Operations Research, 2022, vol. 70, no. 3, pp. 1465-1484, © 2022 INFORMS

Yanfeng Ouyang is George Krambles Endowed Professor at the University of Illinois at Urbana-Champaign. His research focuses on modeling transportation, logistics, and infrastructure systems, and applications to energy, military, and agricultural industries. His work has been recognized by a Walter L. Huber Research Prize from the American Society of Civil Engineers, and a Faculty Early Career Development Award from the U.S. National Science Foundation, among others.

Ruifeng She is a PhD student in civil engineering at the University of Illinois at Urbana-Champaign.